The Influence of Oceanic Barrier Layers on Tropical Cyclone Intensity as Determined Through Idealized, Coupled Numerical Simulations

James Hlywiak*, and David S. Nolan

University of Miami Rosenstiel School of Marine and Atmospheric Sciences, Miami, FL

**Corresponding author address:* 4600 Rickenbacker Causeway, Miami, FL.

E-mail: jhlywiak@rsmas.miami.edu

Early Online Release: This preliminary version has been accepted for publication in *Journal of the Physical Oceanography*, may be fully cited, and has been assigned DOI 10.1175/JPO-D-18-0267.1. The final typeset copyedited article will replace the EOR at the above DOI when it is published.

ABSTRACT

The connection relating upper ocean salinity stratification in the form of oceanic barrier layers to tropical cyclone (TC) intensification is investigated in this study. Previous works disagree on whether ocean salinity is a negligible factor on TC intensification. Relationships derived in many of these studies are based on observations, which can be sparse or incomplete, or uncoupled models, which neglect air-sea feedbacks. Here, idealized ensemble simulations of TCs performed using the Weather Research and Forecasting model (WRF) coupled to the 3D Price-Weller-Pinkel (PWP) ocean model facilitate examination of the TC-upper ocean system in a controlled, high-resolution, mesoscale environment. Idealized vertical ocean profiles are modelled after barrier layer profiles of the Amazon-Orinoco river plume region, where barrier layers are defined as vertical salinity gradients between the mixed and isothermal layer depths. Our results reveal that for TCs of category 1 hurricane strength or greater, thick (24-30 m) barrier layers may favor further intensification by 6-15% when averaging across ensemble members. Conversely, weaker cyclones are hindered by thick barrier layers. Reduced sea surface temperature cooling below the TC inner core is the primary reason for additional intensification. Sensitivity tests of the results to storm translation speed, initial oceanic mixed layer temperature, and atmospheric vertical wind shear provide a more comprehensive analysis. Lastly, it is shown that the ensemble mean intensity results are similar when using a 3D or 1D version of PWP.

Accepted for publication in *Journal of Physical Oceanography*. DOI 10.1175/JPO-D-18-0267.1.

1. Introduction

Air-sea exchanges of enthalpy are a driving force in the evolution of tropical cyclones (TCs) around the globe. These fluxes are a function of the local surface temperature difference between the sea surface temperatures (SSTs) and the temperature of the atmospheric boundary layer, as well as the magnitude of the wind speed on the ocean surface (Ooyama 1969; Price 1981; Bister and Emanuel 1998; Shay et al. 2000). Strong TC cyclonic wind stresses at the air-sea interface induce significant mixed layer current shear, leading to the entrainment of cooler, sub-thermocline waters towards the surface. Thus, a negative feedback arises, since cooling of the sea surface decreases enthalpy fluxes into the storm, limiting the TC potential intensity (Price 1981; Emanuel 1986; Shay et al. 1989; Jacob et al. 2000). For this reason, the underlying structure of the upper ocean beneath the surface layer is often more indicative of how the SST field will evolve under a passing TC than SSTs alone (Leipper and Volgenau 1972; Price 2009).

The magnitude of TC-induced mixing that occurs is related to the density profile of the upper ocean, since regions that are highly stratified within the first few hundred meters are more resistant to sea surface cooling than weakly stratified regions (Price et al. 1986; Shay and Brewster 2010; Vincent et al. 2014). Both temperature and salinity contribute to the density profile of the upper ocean, thus complete knowledge of the upper ocean density profile requires understanding of not only how both temperature and salinity vary vertically and horizontally. This distinction becomes key for certain regions frequently host to TCs, when layers of strong salinity gradients between the iosthermal and mixed layer depths, called ”barrier layers”, contribute significantly to the density profile of the upper ocean (Sprintall and Tomczak 1992; Mignot et al. 2007; Vincent et al. 2014).

Sprintall and Tomczak (1992) is one of the earliest accounts of global tropical oceanic barrier layer regions. Barrier layers are created when the isothermal and mixed layer depths decouple

Accepted for publication in *Journal of Physical Oceanography*. DOI 10.1175/JPO-D-18-0267.1.

mainly due to significant freshening of the surface waters, which can occur down to depths of a few tens of meters from the surface (Lukas and Lindstrom 1991; Pailler et al. 1999; Ffield 2007; Rudzin et al. 2017). Expansive regions of surface freshwater signatures often indicate the presence of a sub-surface barrier layer region, and feature higher stratification than the surrounding waters. One well-documented area where this process occurs is the Amazon-Orinoco freshwater river plume region, where freshwater river runoff from the Amazon and Orinoco river deltas is transported northward into the Caribbean and eastward across the Atlantic's main development region for hurricanes (Pailler et al. 1999; Ffield 2007; de Boyer Montégut et al. 2007; Reul et al. 2014b).

Whether strong salinity stratification favors TC intensification is debated in the literature. Several studies show that interactions with barrier layer regions lead to more active TC seasons (Balaguru et al. 2012; Mignot et al. 2012; Grodsky et al. 2012; Neetu et al. 2012; Reul et al. 2014a; Androulidakis et al. 2016; Yan et al. 2017; Rudzin et al. 2018). Balaguru et al. (2012) was motivated by the passing of Hurricane Omar (2008) over a barrier layer regime near Puerto Rico. During this time, surface cooling was greatly reduced, which may have contributed to an increase in Omar's intensity. Citing statistical data over a decade of TCs across the globe and simulations from a coupled regional climate model, it was found that TCs that passed over barrier layer regions showed increased intensification by a rate of roughly 1.5 times on average, compared to over the open ocean. Through satellite and *in-situ* observations, Reul et al. (2014a) revealed that reductions in cooling over barrier layer regions in the Western Atlantic vary based on TC intensity and translation speed, with the least cooling occurring for slow-moving major hurricanes. Mignot et al. (2012) showed that in the summer months, incoming shortwave radiation warms the barrier layer at a greater rate than the overlying mixed and surface layers, creating sub-surface tempera-

Accepted for publication in *Journal of Physical Oceanography*. DOI 10.1175/JPO-D-18-0267.1.

ture maxima and increased ocean heat contents. In Mignot et al. (2012), as in Reul et al. (2014a), the Western Atlantic is the region of focus.

Newinger and Toumi (2015) agree that the potential presence of sub-surface temperature maxima would limit SST reductions and favor intensification for intense TCs. However, they argue that the presence of biological and inorganic matter in the Western Atlantic block incoming solar radiation from penetrating through the base of the mixed layer, negating the possibility of the formation of sub-surface temperature maxima within the barrier layer. Hernandez et al. (2016) use a regional ocean model to show that sea surface cooling underneath TCs is reduced in this same region, however increased upper ocean stability is to first order a result of thermal gradients, not the salinity profile. Yan et al. (2017) use an uncoupled, 1D ocean model and reasoning from a statistical analysis of TCs in the Western Equatorial Pacific to show that thick barrier layers can actually weaken a storm, if the surface wind stress isn't strong enough to break through the mixed layer.

The goal of this study is to evaluate how barrier layers in the upper ocean modulate air-sea interactions beneath a TC, and how this in turn affects storm intensification. Results from the above studies show that there is high uncertainty regarding the connection between salinity stratification and TC intensification. Most of the aforementioned studies rely on observations, from which it can be difficult to attribute direct cause and effect relationships, uncoupled models, which neglect air-sea feedbacks, or low-resolution model simulations, which don't adequately resolve the TC inner core. Here, we provide a different approach to the problem by directly exploring the evolution of the TC-upper ocean system using a coupled atmosphere-ocean model in a controlled, high-resolution idealized framework. Additionally, sensitivities to the storm translation speed and ability of the environment to favor intensification will be tested. Lastly, results from a

Accepted for publication in *Journal of Physical Oceanography*. DOI 10.1175/JPO-D-18-0267.1.

1-dimensional version of the ocean model will be compared to the results from the 3-dimensional version to weigh the relative roles of upwelling versus mixing towards modifying the barrier layer.

2. Methods

a. Model Description

Numerical simulations were performed using the Weather Research and Forecasting (WRF) Model version 3.9.1.1. WRF provides the option to couple the atmospheric model to the 3-dimensional Price-Weller-Pinkel (3DPWP) ocean model, enabled for this study. In 3DPWP, changes in the vertical structure of the ocean occur due to advection, mixing, and surface heat fluxes. Horizontal dissipation is assumed to be negligible in this study. 3DPWP initiates mixing of the water column when critical bulk and gradient Richardson number criteria are met. Specific details of the model physics are found in Price et al. (1986) and Price et al. (1994).

For each simulation, a low-level atmospheric vortex was initialized following the point-downscaling (PDS) method of Nolan (2011). This method allows the user to set an initial vertical wind shear profile and atmospheric temperature profile that is homogenous across the model domain, without the meridional temperature gradients that would normally be required to balance the atmospheric flow. Each simulation was performed using a fixed outer domain (d01) on an f-plane at 15°N with doubly periodic boundary conditions and a horizontal grid spacing of 18 km, over 320x240 grid points in the zonal and meridional directions. Two fully interactive, nested domains (d02 and d03) in the ocean and atmosphere allowed for finer resolutions of 6 and 2 km over square grids of 180x180 and 240x240 points centered on and moving with the vortex. Timesteps for each atmospheric domain were set to $30, 10$, and 5 seconds for d01, d02, and d03. The ocean timestep was set to 1 minute. Each simulation was integrated for 6 days, and output was saved every 1

Accepted for publication in *Journal of Physical Oceanography*. DOI 10.1175/JPO-D-18-0267.1.

hour. The atmospheric model used 40 equally spaced vertical levels using the WRF pressure coordinates, with the model top at 20 km. The ocean model was comprised of 30 vertical levels separated by a Δz of 6 m from the first model level of 2 m down to 104 m, and a Δz of 16 m below that to a depth of 296 m.

The atmospheric thermodynamic vertical profile was based on the moist tropical sounding of Dunion (2011). The mean flow featured a horizontally homogenous easterly flow, for which the value of the surface velocity was set at run-time The background flow was maintained throughout the duration of each simulation using the Time-Varying PDS (TVPDS) feature, developed by Onderlinde and Nolan (2017). TVPDS has been used previously to nudge the large-scale atmospheric environment towards a second (or more) prescribed state, to realistically represent the passage of a TC from one environment into another. In this study, this technique was used to nudge the atmospheric environment towards the initial state over a time-scale of 24 h, applied to the outermost domain only (not including grid points overlapping with d02 and d03). The application of this technique here forced the simulated TC to track westward, minimizing meridional shifts in track due to interactions between the TC and the TC-induced shear, without compromising the model's ability to replicate realistic TCs. The radius of maximum winds (RMW) and maximum 10 meter wind speed (VMAX) of the initial vortex were 90 km and 21.8 m s^{-1}. Ensembles of simulations were produced by adding small asymmetries to the initial vortex wind field. For each set of controlling parameters, 5 ensemble members were produced. The most current WRF drag and enthalpy exchange coefficient schemes are outlined in Dudhia et al. (2008), for which the drag coefficient saturates at high wind speeds. WSM5 microphysics and the YSU boundary layer scheme were used. Shortwave and longwave radiation schemes were turned off across all domains, to filter out the effects of the diurnal cycle.

Accepted for publication in *Journal of Physical Oceanography*. DOI 10.1175/JPO-D-18-0267.1.

To test the sensitivity of the results to different background environments and base storm intensities, three different environment sets were created by slightly varying initial atmosphere and ocean conditions. This facilitated comparisons of how the TC-barrier layer connection changes due to differences in the favorableness of the environment towards TC intensification, providing a more comprehensive analysis. These will be referred to as the un-favorable (UNFAV), moderately-favorable (MOD), and favorable (FAV) ensemble sets. In UNFAV and MOD, the surface-to-model top bulk vertical wind shear is set to 7.5 m s^{-1} and the isothermal layer temperature is set to 27°C for UNFAV and 28°C for MOD. In the FAV set, these values are 5 m s^{-1} and 29°C. Further details about the environmental initialization will be described in the following sections, 2b and 2c.

b. Atmospheric Experimental Cases

Numerous studies show that the response of the ocean to a passing TC depends greatly on the size, intensity, and residence time of the wind forcing (Price 1983; Shay et al. 1989; Samson et al. 2009; Yablonski and Ginis 2009; Reul et al. 2014a). To test the sensitivity of the results to the latter, simulations were repeated using different storm translation speeds. The storm motion depends on the environmental steering flow, which was created based on the large-scale surface winds and bulk vertical shear values. Therefore, altering the translation speed for a given shear value required a change in the mean environmental easterly steering flow through the surface easterly wind speed values. These surface values were 4 and 6 m s^{-1} for UNFAV, 4, 6, and 8 m s^{-1} for the MOD set, and 3.5 and 6 m s^{-1} for the FAV set. These will be collectively referred to as SLOW, MEDIUM, and for MOD only, FAST. Due to the complex evolution of coupled simulations from the point of initialization, and the fact that the atmospheric steering flow felt by the TC changes as the storm intensifies, slight variations in motion were unavoidable over each 6 day integration. Therefore, the time-mean of two non-dimensional numbers were employed to

Accepted for publication in *Journal of Physical Oceanography*. DOI 10.1175/JPO-D-18-0267.1.

diagnose the translation speed, both functions of the translation speed U_h, in units of m s $^{-1}$. U_h was determined every 15 minutes using 2nd order centered difference calculations of TC center positions. The TC center was calculated by finding the pressure centroid following the method of Nguyen et al. (2014), rounded to the nearest d03 grid point.

The first number, $C = U_h/fL$, in which f is the Coriolis parameter and $L = 100$ km, a characteristic length scale for TCs, is the horizontal aspect ratio of the ocean SST response (Price 1983; Greatbatch 1984). The parameter appears in Lloyd and Vecchi (2011), where it is shown that ocean SST responses are greatest for $C \leq 1$ and diminish for greater values. The second non-dimensionalized number is $S = \pi U_h/4fR$, in which f is as before and R is the instantaneous surface RMW. S is the ratio of the local inertial frequency to the near inertial frequency provided by the wind stress curl (Price 1983). For $S = 1$, the right-of-track SST cooling due to mixing underneath the TC is maximized.

Examples of ensemble mean C, S, and U_h from MOD SLOW, MEDIUM, and FAST are shown in Fig. 1. Mean values for each case were roughly $C = 0.5, 1$, and 1.5, and $S = 1, 2$, and 3. These values are consistent between UNFAV, MOD, and FAV, as well as between ensemble members of each set. An overall slight decreasing trend in these values is due to the response of the TC vortex to deeper levels of westerly shear as the vortex penetrates further upward into the troposphere with time. S shows the steepest decline in time, which could have a slight impact on cooling due to mixing at the end of the simulation period. However, this is mostly due to changes in the RMW, and S is consistent up until the point of TC lifetime maximum intensity (LMI), to be discussed in section 3. Based on these values, with all else being equal, SLOW should theoretically result in the greatest vertical mixing and upwelling and FAST should force the smallest SST response. For brevity, in the discussions below with the exception of section 3c, the MOD, FAST set will be excluded, as the results showed minimal dependence on the state of the underlying ocean.

Accepted for publication in *Journal of Physical Oceanography*. DOI 10.1175/JPO-D-18-0267.1.

c. Ocean Temperature and Salinity Profiles

The upper ocean temperature and salinity profiles were constructed at the moment of model initialization. The initial ocean was quiescent, i.e. featuring no initial currents or sea surface height anomalies (height anomalies are not calculated through 3DPWP). Each simulation was initialized using one of three different temperature and one of four different salinity profiles; one featuring constant salinity and three barrier layer cases of varying thicknesses. Figure 2 shows the three temperature profiles used, along with salinity, density, and squared Brunt-Väisälä frequency profiles for each barrier layer case for the MOD temperature profile. Barrier layer thickness is defined as the difference in the isothermal and mixed layer depths (ILD and MLD, respectively). Here, as in de Boyer Montégut et al. (2007), the former is defined as the model level at which the temperature deviates from the 10 m temperature by $\Delta T = 0.2°\mathrm{C}$, and the later as the depth at which the potential density σ exceeds the 10 m σ by the same amount that it would for a temperature decrease of the same ΔT for a constant salinity profile, i.e. $\Delta\sigma$ shown in equation 1, rounded up to the nearest model level.

$$\Delta\sigma = \sigma(T - \Delta T, S, P) - \sigma(T, S, P) \tag{1}$$

The constant salinity case, OBL0, features initial salinity values of 36 psu at every model level. Hyperbolic tangent functions were used to create the variable salinity profiles, allowing for a smooth and realistic increase in salinity with depth resulting from varying strengths of surface freshwater inputs. The three barrier layer cases featured layer thickness of $12, 24$, and 30 m, which were constructed by changing the coefficients of the hyperbolic tangent function. These cases will be referred to as OBL12, OBL24, and OBL30 from here on out (these comprise the OBLx cases, in contrast to the OBL0 case). Initial sea surface salinity values for each were $35.39, 33.84$, and

Accepted for publication in *Journal of Physical Oceanography*. DOI 10.1175/JPO-D-18-0267.1.

31.32 psu. In every simulation, the initial temperature is constant down to the ILD, located at 50 m (27, 28, and 29°C for UNFAV, MOD, and FAV, respectively). Below this, the temperature decreases at a lapse rate of 0.1°C m^{-1}. Because salinity stratification is the primary focus here, pre-passage conditioning of the vertical temperature distribution within the barrier layer due to incident solar radiation was not considered. Temperature, salinity, and barrier layer thickness values most closely resemble observations within the Amazon-Orinoco plume region (Pailler et al. 1999; Ffield 2007; de Boyer Montégut et al. 2007; Foltz and McPhaden 2009). However, barrier layer profiles observed for other regions of the global tropical ocean, such as the Western Pacific or the Bay of Bengal, feature similar characteristics (Mignot et al. 2007; Neetu et al. 2012; Yan et al. 2017).

Finally, SLOW cases were repeated for MOD and FAV using a 1D representation of PWP (1DPWP). In 1DPWP, ocean model grid points communicate only in the vertical direction, thus removing the influence of horizontal and vertical advection. This serves to elucidate the roles of 3D processes in modulating the upper ocean structure.

As shown in table 1, in total, 4 barrier layer, 2 U_h (with additional MOD, FAST simulations), and 3 initial isothermal layer temperature scenarios were integrated forward 5 times using different initial vortices to create an ensemble for each case, resulting in 140 simulations using 3DPWP. Additionally, 1 U_h, 2 initial isothermal layer temperatures, 4 barrier layer cases, and 5 ensemble members coupled to 1DPWP resulted in a total of 180 unique simulations.

3. Results From 3D Ocean Simulations

TC evolution across every simulation was similar, in that a spin-up period of a day or two was required before varying degrees of intensification occurred. Figure 3 shows an example evolution of the model-derived 10 cm radar reflectivity field for a MOD, MEDIUM ensemble member, at $t = 24, 72, 120$ and 144 h of integration time, plus sample tracks from one SLOW, MEDIUM, and

Accepted for publication in *Journal of Physical Oceanography*. DOI 10.1175/JPO-D-18-0267.1.

FAST ensemble member from MOD. The reflectivity plots show that the simulations produced realistic TC features such as a clear eyewall fully wrapping around the eye by $t = 120$ h and the development of outer rain bands. These characteristics were common to nearly every simulation. While differences between the tracks of each U_h case are clear, track was seemingly independent of the barrier layer thickness (not shown). Hereafter, it is assumed that the presence of the barrier layer plays little direct impact on the track of a TC, other than slight wobbles due to intensity differences.

a. Intensity Sensitivity to Non-Barrier Layer Related Factors

Before discussing sensitivities to salinity stratification, it is important to acknowledge sensitivities of the TC intensity across all barrier layer cases to changes in translation speed, initial isothermal layer temperature, and the large-scale vertical wind shear. Time-series plots of ensemble mean VMAX in fig. 4 and 5 show the TC intensity evolution. These simulated TCs evolve similarly to observed cyclones in nature that originate from initially weak disturbances. At $t = 24$, when all TCs were the equivalent of strong tropical storm or weak category 1 hurricane intensity on the Saffir-Simpson scale, weakening occurs as SST cooling increases, regardless of environment. Differing rates of steady intensification occur after this point as the enthalpy flux into the storm recovers. Additionally, LMI was reached at roughly $t = 100 - 120$ h for UNFAV and MOD, and between $t = 72 - 96$ h for FAV. TCs in the UNFAV set achieve strong category 2 designation (VMAX ≈ 45 m s^{-1}) by the end of the simulation time-frame, while the MOD (FAV) TCs reached intensities at the lower (higher) end of category 3 designation (VMAX ≥ 50 m s^{-1}). Additionally, VMAX for UNFAV, MEDIUM appear to be stronger than UNFAV, SLOW, however subtracting the motion vector from the surface wind speed shows that there is no difference between MEDIUM

Accepted for publication in *Journal of Physical Oceanography*. DOI 10.1175/JPO-D-18-0267.1.

and SLOW (not shown). For FAV, subtracting the motion vector from VMAX didn't change the differences between SLOW and MEDIUM.

There were noticeable differences in TC intensity evolution between the UNFAV, MOD, and FAV simulations. Although VMAX is a better proxy than most intensity metrics for the response of the upper ocean to the simulated TCs, this metric was fairly volatile in time. Therefore, most of the following analysis comparing simulations will focus on the much more consistent surface minimum pressure (PMIN), which is especially valid since the TCs are all about the same size and occur at the same latitude. Figures 6 and 7 show time series plots of PMIN comparing the three environments for SLOW and MEDIUM (solid lines, right axis).

Differences in TC evolution between environments was greatest for SLOW. For these SLOW cases, the early spin up period was reduced for increasing environmental favorableness, and steady intensification occurred sooner. The more favorable the environment, the greater the LMI; the FAV set generally intensified to PMIN values of roughly 950 hPa by $t = 80$ h, while the mean UNFAV intensities at $t = 80$ h were roughly 995 hPa, reaching a maximum between $970 - 975$ hPa by the end of the simulation time period. In MOD and FAV, weakening occurred after reaching LMI.

PMIN differences between MEDIUM environments were less pronounced. Similar to FAV, SLOW, the FAV, MEDIUM set produced the strongest storms, as values of PMIN for the ensemble mean OBL24 and OBL30 cases were close to 940 hPa and values for the OBL12 and OBL0 were roughly 950 hPa. UNFAV, MEDIUM resulted in TCs that intensified sooner, thanks to a decrease in residence time over the marginal ocean environment. LMI values between $965 - 970$ hPa for all barrier layer cases occurred for UNFAV. Unlike for SLOW, MEDIUM TCs across all environments generally plateaued in intensity after reaching LMI instead of weakening, despite the slight reduction in U_h at later times (fig 1).

Accepted for publication in *Journal of Physical Oceanography*. DOI 10.1175/JPO-D-18-0267.1.

Ensemble member variation from the ensemble mean also depended on U_h and environmental favorableness. Also shown in fig. 6 and 7 are time-series of the spread in ensemble member standard deviation from the ensemble mean for each UNFAV, MOD, and FAV barrier layer case (dashed lines, left axis). It appears that the period of highest ensemble member variability begins at the onset of intensification and ends when intensification slows, occurring sooner for increasing environmental favorableness. Ensemble member spreads during these intensification phases were greatest for the UNFAV and MOD sets, and generally increased for increasing barrier layer thickness. The FAV, SLOW set displayed very little spread among ensemble members, suggesting that the more favorable the environment is for TC development, the higher the predictability of strong TCs during intensification periods. The members of each case converge to the mean value by the end of day 6, roughly the timing of LMI.

To summarize this sub-section, all ensemble means produced similar intensification rates. However, TCs in the MOD and FAV set began intensifying sooner than in UNFAV and reached stronger LMIs, with FAV producing the strongest storms. SLOW TCs were more vulnerable to weakening towards the end of the 6-day simulation period. It will be shown in the next section that the end of the intensification phase correlates with the erosion and deepening of the barrier layer underneath of the storm. Additionally, ensemble member variations in intensity was largest mid-way through the simulation, due to differing timing of the onset of intensification.

b. Upper Ocean Evolution due to Barrier Layer Thickness

The SST response depends strongly on the TC intensity, U_h, and also the barrier layer thickness. The local temporal and spatial scales in which ocean structural changes are studied here indicate that cooling is primarily a response due to the direct forcing of the wind field (Shay et al. 1989; Price et al. 1994). Thus, the assumption here is that further cooling at longer timescales due to

Accepted for publication in *Journal of Physical Oceanography*. DOI 10.1175/JPO-D-18-0267.1.

near-inertial oscillations that persist after storm passage has little influence on intensity changes. This relaxation stage of cooling due to near-inertial oscillations would have an impact on successive TC passages over the region, but this is beyond the scope of this study.

Several studies indicate that air-sea fluxes well beyond the RMW affect storm structure (Cione and Uhlhorn 2003; Xu and Wang 2010; Sun et al. 2014). Cione and Uhlhorn (2003) and Yablonski and Ginis (2009) define 60km and 200km as estimates of the inner core and the outer core containing the cold wake, and changes in air-sea fluxes within both radii may significantly impact the TC. Time-series of ensemble mean SST changes averaged within 60 (solid lines) and 200 (dashed lines) km of the storm center are shown in Figures 8 and 9. Note that the above ensemble mean values are axisymmetric, and do not account for storm asymmetries. Additionally, variations in the ocean responses between ensemble members were much smaller than variations in TC intensity (not shown).

Inner core SSTs fall steadily in time. Additionally, the trends in the 200 km plots are similar to the 60 km plots. The magnitude of cooling increases for decreasing U_h; as much as 3°C within 60 km for SLOW TCs occurs at $t = 140$ h compared to less than 1.5°C for MEDIUM storms. Storms embedded within FAV show the greatest cooling, in part because the TCs within this set are the strongest and thus induce more entrainment mixing across the ILD. Cooling for the FAV, SLOW simulations plateaus just before 96 hours, coinciding with the end of the intensification stage for this set, indicating that a quasi-steady state is reached.

Figures 10 and 11 reframe the OBLx 60 km plots relative to the OBL0 cooling, to show the influence of salinity gradients on SST changes. An interesting reversal in the trends between SST cooling and barrier layer thickness arises as a function of time. Initially, increasing barrier layer thickness leads to increased cooling. The duration of this period depends on U_h and the environment, but generally occurs from $t = 0 - 24$ h for SLOW and $t = 0 - 48$ h for MEDIUM.

Accepted for publication in *Journal of Physical Oceanography*. DOI 10.1175/JPO-D-18-0267.1.

Although the mean differences during this period appear to be small (on the order of 0.01°C), the relationship is robust across all simulations. During the intensification phase, as intensities exceed category 1 status, increased cooling is observed for thinner barrier layers, by over 0.5°C greater for the OBL0 cases compared to the OBL30 cases. By the end of the 6 day period, the SLOW barrier layer ensemble means show convergence, but generally plateau for MEDIUM. By the end of the simulation time, cooling between these SLOW barrier layer ensemble means was nearly similar while cooling for MEDIUM varied more significantly between barrier layer cases. By $t = 144$ h, differences in average cooling reach up to $0.8-1$°C within 60 km for MEDIUM, while for SLOW, final cooling values are similar between barrier layer cases.

The early reversal in ΔSST trends as a function of barrier layer thickness helps elucidate how the upper ocean structure is modified over time when an barrier layer is present. Figure 12 shows cross-sections of ocean temperature at constant latitudes intersecting the storm center for a MOD, MEDIUM case, confirming that the mixed layer cools slightly more for thicker barrier layers early on. At $t = 20$ h (fig. 12(a-d)), mixing across the isothermal layer in the OBL0 case has already occurred close to the TC center, while in the OBLx cases, vertical mixing is confined to the top of the halocline. At this time, SSTs are lower by $0.1-0.2$°in the OBLx cases, and the warmest waters are trapped within the bottom of the barrier layer, just above the ILD, creating a sub-surface temperature maximum. At $t = 80$ h, waters from below the ILD have been entrained into the surface layer for all barrier layer cases, and SSTs in the vicinity of the center are warmer as barrier layer increases. The sub-surface temperature maximum layer at the edge of the domain ahead of the storm in the OBLx cases indicates that the barrier layer is still present at large radii away from the storm center where mixing is weaker, and that the mixed layer still has the potential to warm as the storm continues to track westward. The observed evolution of the barrier layer follows what was hypothesized by Yan et al. (2017) and supports suspicions that the presence of thick barrier

Accepted for publication in *Journal of Physical Oceanography*. DOI 10.1175/JPO-D-18-0267.1.

layers can actually lead to increased SST cooling for weaker wind stresses. In the scenario of a weak wind forcing, the energy within the shallow mixed layer is depleted more rapidly, leading to a sub-surface temperature maximum layer as the warmer waters within the halocline remain unperturbed or trapped below the MLD.

Beyond this early cooling period, the simulations for which a barrier layer is present feature warmer mixed layers. Figure 13 shows time-depth plots of the temperature and salinity profile beneath a point following the TC center for MOD, MEDIUM and FAV, MEDIUM ensemble members, focusing on OBL0 and OBL30. For both members, the OBL30 mixed layer is warmer than the OBL0 mixed layer by several tenths of a degree. Additionally, cooling is accompanied by the deepening and erosion of the barrier layer, shown as the difference in the MLD (white lines) and ILD (black lines).

Figure 14 shows the difference in SST between a MOD, OBL30 and OBL0 ensemble member at three different times, for both SLOW and MEDIUM. Most noticeably, SSTs behind the TC (and within $2-3$ RMW at $t = 80, 120$ h) where barrier layer erosion has occurred or is still in progress are warmer in the OBL30 case by up to 2°C. Meanwhile, temperatures ahead of and at large radii away from the center where the barrier layer remains unperturbed are warmer in the OBL0 case by less than 0.5°C. This again confirms that when the TC wind forcing is weak, thicker barrier layers lead to slightly greater SST cooling. The opposite is true when the wind forcing is sufficiently strong. This indicates that weak TCs passing over barrier layer regions that fail to reach this wind forcing threshold may experience a delay in intensification until mixed layer shear is strong enough to initiate entrainment of warm barrier layer waters into the mixed layer. Additionally, the SLOW SST field at $t = 120$ h shows greater cooling within 1 RMW of the average storm center position than in the MEDIUM SST field. This indicates that barrier layer erosion is completed by the end of the simulation period, and the sub-surface temperature maximum layer underneath the

Accepted for publication in *Journal of Physical Oceanography*. DOI 10.1175/JPO-D-18-0267.1.

TC around 1 RMW has been well-mixed throughout the column, so that increased cooling picks up again in Figure 10. This explains why the SLOW TCs tended to weaken after achieving their LMI.

These results lead us to consider the question, at which intensity threshold do the barrier layer cases begin to feature less cooling than the constant salinity case? This as well depends on U_h, barrier layer thickness, and how favorable the environment is for TC development. Figure 15 shows the times at which the ensemble mean OBL0 60 km SST cooling first equaled or exceeded the cooling for the ensemble mean OBLx ((a),(b)), the VMAX at these times ((c),(d)), and PMIN at these times ((e),(f)) for SLOW ((a),(c),(e)) and MEDIUM ((b),(d),(f)). This figure shows that for a given barrier layer thickness, increasing the environmental favorableness decreased the time it took for the SST reversal to occur, likely due to differences in intensity. The ensemble mean intensities at these times were slightly below category 1 status (33 m s^{-1}) Additionally, thicker barrier layers required higher intensities before the SST trend reversal occurred. Finally, differences in these values for SLOW were less sensitive to environmental favorableness and barrier layer thickness.

c. TC Intensity Changes Related to Barrier Layer Thickness

The sensitivities of TC intensity to salinity stratification will now be discussed. Figures 16 and 17 show the ensemble mean PMIN plots from fig. 6 and 7 relative to OBL0. The MOD and FAV sets produced the greatest differences between OBLx cases, likely owing to the greater intensities for those sets compared to UNFAV (refer back to Figure 6 and 7). Differences in PMIN for FAV, SLOW and FAV, MEDIUM, were as large as 7 hPa between OBL0 and OBL30, and roughly 4 hPa between OBL0 and OBL30 for the MOD, SLOW and MOD, MEDIUM. Additionally, increasing spread between the mean intensities occurs mainly during the intensification phase. By day 5 or 6, depending on the environment, the mean intensities generally plateau relative to each other. This

Accepted for publication in *Journal of Physical Oceanography*. DOI 10.1175/JPO-D-18-0267.1.

provides more evidence that the barrier layer is most influential on intensity changes between the time when mixing is limited to above the ILD up to when mixing across the ILD occurs.

The initial OBLx SST cooling period during the first 48 hours seemed to have little effect on intensity for MEDIUM. Conversely, in MOD, SLOW and FAV, SLOW, weakening of OBLx by as much as 4 and 2 hPa are clear at 50 and 25 h for OBL24 and OBL30. In MOD, SLOW this lags the timing of the initial cooling by about a day, while there appears to be no lag for FAV, SLOW. Whether a lag is present or not, this slight weakening of the OBLx cases occurs early during the intensification phase for all environments.

Differences in enthalpy flux (latent plus sensible heating) into the atmosphere between OBLx cases help explain these intensity trends. Figure 18 shows the ensemble mean azimuthally-averaged enthalpy flux as a function of RMW away from the center for SLOW MOD at three different times: $t = 50, 80$, and 120 h. At $t = 50$ h, the flux is almost equivalent at the RMW, but is slightly larger for decreasing barrier layer thickness, lagging the reversal in the SST response by several hours. Later, enthalpy at the RMW increases for increasing barrier layer thickness by ≈ 100 W m^{-2}, especially between 1-3 RMW, where SST cooling is maximized (refer to Figure 14). Additionally, the increased flux for the OBLx cases appears to occur first near the RMW and spreads out to larger radii in time, as greater OBLx fluxes are confined within 2.5 RMW at $t = 80$ h but exceed 4 RMW at $t = 120$ h.

The aforementioned lag between the early OBLx weakening and SST cooling, most noticeable for MOD SLOW, may be explained through the formulae for air-sea exchanges of heat and momentum. Air-sea parameterizations of these exchanges are proportional to the wind stress at the interface, thus differences in the flux into the atmosphere between barrier layer cases will be less sensitive to differences in barrier layer SST cooling when winds are relatively weak, with all else being equal (Price 1981). VMAX is mostly below hurricane status during the early phase for

Accepted for publication in *Journal of Physical Oceanography*. DOI 10.1175/JPO-D-18-0267.1.

which SSTs were warmer for increased thickness (fig. 4 and 5). Delays are less noticeable for later times and for the FAV simulations, i.e. stronger wind stresses. This leads to the hypothesis that for situations in which intensity increases in time, the initial phase during which OBL0 experiences the least amount of cooling has less of an influence on TC intensity changes when the base intensity is weak. However, for already strong TCs entering a thick barrier layer region marked by a surface salinity front, this initial cooling reversal phase could have a more immediate impact on enthalpy fluxes before the MLD is deepened and warmer waters are entrained towards the surface.

The above intensity analysis is fairly qualitative, but shows that for TCs of strong tropical storm or hurricane status, increasing salinity stratification aids further intensification. To condense the overall sensitivity to salinity into a single metric for easier comparison, a barrier layer index (OBLI) was computed for every ensemble member of every case, shown in equation 2. OBLI compares the LMI of the OBLx cases compared to the OBL0 cases, defined as the difference between LMI defined by PMIN and the initial intensity, multiplied by 100 to yield a percentage.

$$OBLI = \frac{\Delta I_{OBLx} - \Delta I_{OBL0}}{\Delta I_{OBL0}} * 100 \tag{2}$$

OBLI was computed for each OBLx ensemble member of every simulation performed. Figure 19 shows the ensemble OBLI, with linear trend lines and r^2 values provided. Additionally, Table 2 lists the ensemble means and standard deviations for each case. There is a lot of variance in the data, however, several relationships stand out. First, the presence of the barrier layer aids in increasing LMI, i.e. an overwhelming majority of OBLI ensemble member values are greater than zero. Second, increasing thickness generally leads to an increase in OBLI. Third, the ensemble UNFAV, SLOW OBL30 mean values are the largest, with a mean value of 15.82% versus 12.12% and 10.11% for MOD, SLOW and FAV, SLOW OBL30. The opposite trend occurs for MEDIUM, as mean values increase from UNFAV to FAV OBL30, from $6.64 - 9.68\%$. Fourth, r^2 values are

Accepted for publication in *Journal of Physical Oceanography*. DOI 10.1175/JPO-D-18-0267.1.

greatest for MOD, MEDIUM and FAV, MEDIUM, with values of 0.55 and 0.48 for MOD and FAV. Low correlation between thickness and OBLI exists for SLOW and FAST storms, with r^2 values between 0.15 – 0.20 for SLOW in all environments, and 0.10 for MOD FAST. Therefore, this data suggests that the influence of the barrier layer is most consistent for a medium U_h regime, around 4 m s^{-1}. The large mean OBLI value and low correlation for the slowly translating TCs - roughly 2 m s^{-1} - suggests that the potential increase in intensification due to the presence of the barrier layer is greatest for SLOW storms embedded within marginal environments, but is a secondary influence on the intensity of these TCs compared to wind shear and initial mixed layer temperature.

In theory, OBLI should be a measure of what percentage of the intensity change is due directly to the presence of barrier layers of varying thickness, where positive (negative) percentages would indicate that the barrier layer favors (suppresses) intensification. Due to the high level of complexity associated with coupled simulations, it would be incorrect to assume that the barrier layer is the only factor influencing differences in OBLI. Additionally, OBLI isn't a comprehensive indication of the effects of the salinity stratification on intensity, as the change in intensity is only determined at the time of maximum intensity and fails to describe anything about differences in timing of attaining maximum intensity. However, using an ensemble in this scenario provides a more robust analysis of influence of the barrier layer on the LMI, and the provided r^2 values show how much of the variance in OBLI is due to barrier layer thickness, indicating the consistency in the feedback mechanism.

4. Intensity Sensitivity to Barrier Layer Thickness Using 1DPWP

For observed TCs passing over an oceanic region, the response of the upper ocean structure has a complex, 3-dimensional evolution. When performing coupled numerical simulations, it is often

Accepted for publication in *Journal of Physical Oceanography*. DOI 10.1175/JPO-D-18-0267.1.

useful to approximate this response as 1-dimensional where advection is ignored and only vertical mixing is simulated, with the benefit of reducing computational expenses. Many studies suggest that 1D ocean dynamics are adequate, especially for large spatial domains and resolutions, for which adding horizontal physics result in marginal gains (Bender et al. 2007; Davis et al. 2008). Other studies argue for the necessity of including the full 3D physics, especially for slow moving storms for which upwelling plays a significant role in cooling SSTs (Price et al. 1994; Yablonski and Ginis 2009; Yablonsky and Ginis 2012; Wu et al. 2016). The goal of this section is not to argue against the necessity of including higher order ocean dynamics regardless of computational expense, but to show whether or not the simulated barrier layer response and therefore TC intensity changes depend on which processes are included, and to additionally shed some light towards the role of the barrier layer in modulating the relative roles of entrainment mixing vs upwelling on cooling.

Figure 20 compares the 1D and 3D MOD, SLOW and FAV, SLOW results of the ensemble mean PMIN for each barrier layer thickness (1D simulations were only performed for SLOW). Overall, there is very little difference between the 1D and 3D mean intensities, as the TC evolution is quite similar between the two. The ensemble mean total ΔSST, averaged within 200 km of the center, between the two groups is also nearly identical (solid blue (red) plots of fig. 21 for the 1D (3D)). OBL0 and OBL30 are shown for brevity. ΔSST is separated into two components, a front and a rear average relative to the storm motion, which are the combined averages of the front two and rear two quadrants, respectively. When summed together, the cooling ahead and behind the storm result in the total ΔSST. As the largest cooling occurs behind the storm, the rear plots feature the greatest cooling and lie below the total, which means that the frontal plots must lie above the total. Because upwelling effects are often observed behind and along the storm track, this allows for the closer examination of the effects of upwelling on SST cooling.

Accepted for publication in *Journal of Physical Oceanography*. DOI 10.1175/JPO-D-18-0267.1.

Incidentally, there appears to be little observable difference in the SST field averaged within 200 km between the 1D and 3D simulations. Slight differences are observed at the end of the simulation, although there doesn't appear to be a consistent relationship between the 1D and 3D cooling differences during this time when comparing the different barrier layer and environmental favorableness cases. Averaging within 60 km doesn't change this outcome (not shown). These intensity and SST analyses suggest that the role of 3D ocean mechanisms, mainly horizontal advection and upwelling, play a small role in influencing TC intensity changes in an ensemble mean sense for the configurations used in this study. An alternative explanation is that the simulation time period would need to be extended past 6 days to allow the 3D mechanics to become a more influential factor.

Although the influence on the ensemble mean is small, effects on the ensemble member variance was more pronounced. Referring back to Fig. 19d, it is clear that a much higher correlation is seen between OBLI and thickness when using 1D physics. Although the means are not very different, r^2 values increase from 0.16 to 0.50 for MOD and 0.18 to 0.40 for FAV. Likewise, from table 2, the 1D OBLI means for OBL30 are roughly 1.5% larger, and the standard deviations decrease by half for MOD and by 1.20% for FAV. Additionally, standard deviations between 1D ensemble members are smaller than their 3D counterparts by $1-2$ hPa in fig. 20. The reason for this reduction in volatility remains for future research.

5. Summary

For idealized, coupled simulations based on profiles typically observed in the Amazon-Orinoco freshwater river plume region, the presence of the barrier layer has a stabilizing effect on the upper ocean and reduces entrainment-mixing of cooler, sub-thermocline waters towards the surface. Results here support findings from several previous studies detailed in section 1 that claim that

Accepted for publication in *Journal of Physical Oceanography*. DOI 10.1175/JPO-D-18-0267.1.

oceanic salinity stratification has a non-negligible effect on intensity. The degree to which the barrier layer favors further intensification increases with increasing thickness of the salinity layer, and when averaged over many storms, increases for decreasing translation speed. For TCs moving at or around 2 m s^{-1}, exposure to 30 m thick barrier layers for several days allowed for further decreases in lifetime minimum pressure between $10 - 15\%$, compared to cases featuring constant salinity, albeit with high ensemble member deviation. For storms translating at roughly 4 m s^{-1}, this range was $6 - 10\%$, but the ensemble spread was much lower. Results were most consistent between ensemble members for storms translating in this regime. As this would include a large fraction of storms in the Atlantic (Yablonski and Ginis 2009), the results here have important implications for observed cyclones.

The upper ocean evolution occurs in three stages, similar to what was proposed in Yan et al. (2017). Initially, when a strong barrier layer is present, the shear-induced mixing is too weak to deepen the mixed layer, which is fairly shallow to begin with as the halocline is close to the surface. Heat fluxes draw energy out of the mixed layer, and the cooling rate is enhanced. A subsurface temperature maximum results as the waters within the barrier layer remain unperturbed. Second, if the surface wind stress becomes strong enough to induce mixing through the top of the halocline, warm waters within the barrier layer are entrained into the mixed layer. This results in a stoppage or reduction in surface cooling. Finally, wind stresses may be able to mix through or deepen the barrier layer, and the rate of cooling increases once again. Whether the barrier layer completely erodes away depends on the combination of the storm translation speed and intensity, plus the barrier layer thickness.

While some previous studies suggest that the barrier layer becomes a factor for only the most powerful TCs, the results here suggest that the barrier layer begins to aid intensification when mixed layer current shear is significant enough to mix through the top of the halocline, which

Accepted for publication in *Journal of Physical Oceanography*. DOI 10.1175/JPO-D-18-0267.1.

here occurred for storms of strong tropical storm or low-end category 1 status. For TCs that fail to reach this necessary intensity due to more hostile atmospheric or oceanic conditions, thick barrier layers may enhance mixed layer cooling, thus limiting the storm's potential intensity. On the other hand, for storms above this threshold in more hostile environments, the presence of a thick barrier layer may be enough to prevent or delay TC decay. Clearly, this threshold intensity will change depending on depth of the mixed layer and the thickness of the barrier layer, but the results here suggest that the barrier layer is more likely to aid in the intensification of TCs near and above hurricane status. Additionally, it was found that the influence of the barrier layer is greatest during the time between when mixing breaks through the top of the halocline and the isothermal layer. After this time, intensity differences between the experiments of differing thicknesses mostly plateaued. In this study, longwave and shortwave radiation were turned off. Thus, the sub-surface temperature maxima often observed to be co-located with the barrier layer wasn't initialized before storm passage, and initial ocean heat content values were identical across different barrier layer cases for the same isothermal layer temperature. Including radiation could possibly aid in increased intensification rates than what were observed here, and requires more attention in future studies.

Despite significant advancements in TC track forecasts over the past several decades, intensity forecasts have improved very little. Even a 10% increase in TC intensity attributed to barrier layer interactions significantly increases the destructive force of hazards such as storm surge and wind damage. Thus, the need for identification and improved model representation of factors affecting intensity remain great. In this study, a feature often overlooked in the numerical modelling and forecasting of TCs is found to appreciably affect TC intensification. An advantage of using idealized simulations here is that the physical processes identified can be applied to many regions of the global tropical ocean where barrier layers are common features. Therefore, although the initial

Accepted for publication in *Journal of Physical Oceanography*. DOI 10.1175/JPO-D-18-0267.1.

profiles used in this study were based on observations of the Amazon-Orinoco river plume, the results of this study can apply to regions such as the Eastern Indian and Western Pacific Oceans, where barrier layers are common. However, more work should be done to better place the results here in the context of real-case applications.

Acknowledgments. J. Hlywiak was supported by a University of Miami Graduate Fellowship and D. Nolan was supported by NSF PREEVENTS Track 2 Award 1663947. We thank two anonymous reviewers for their helpful comments.

References

Androulidakis, Y., V. Kourafalou, G. Halliwell, M. Le Hénaff, H. Kang, M. Mehari, and R. Atlas, 2016: Hurricane interaction with the upper ocean in the amazon-orinoco plume region. *Ocean Dynamics*, **66 (12)**, 1559–1588.

Balaguru, K., P. Chang, R. Saravanan, R. L. Leung, Z. Xu, M. Li, and J. S. Hsieh, 2012: Ocean barrier layers' effect on tropical cyclone intensification. *PNAS*, **109 (39)**, 14 343–14 347, URL 10.1073/pnas.1201364109.

Bender, M. A., I. Ginis, R. Tuleya, B. Thomas, and T. Marchok, 2007: The operational gfdl coupled hurricane–ocean prediction system and a summary of its performance. *Monthly Weather Review*, **135 (12)**, 3965–3989.

Bister, M., and K. A. Emanuel, 1998: Dissipative heating and hurricane intensity. *Meteorology and Atmospheric Physics*, **65 (3-4)**, 233–240.

Cione, J. J., and E. W. Uhlhorn, 2003: Sea surface temperature variability in hurricanes: Implications with respect to intensity change. *Monthly Weather Review*, **131 (8)**.

Accepted for publication in *Journal of Physical Oceanography*. DOI 10.1175/JPO-D-18-0267.1.

Davis, C., and Coauthors, 2008: Prediction of landfalling hurricanes with the advanced hurricane WRF model. *Monthly weather review*, **136 (6)**, 1990–2005.

de Boyer Montégut, C., J. Mignot, A. Lazar, and S. Cravatte, 2007: Control of salinity on the mixed layer depth in the world ocean: 1. general description. *Journal of Geophysical Research: Oceans*, **112 (C6)**.

Dudhia, J., and Coauthors, 2008: Prediction of atlantic tropical cyclones with the advanced hurricane WRF (AHW) model. *28th Conference on Hurricanes and Tropical Meteorology*, Am. Meteorol. Soc., Orlando, FL.

Dunion, J. P., 2011: Rewriting the climatology of the tropical north atlantic and caribbean sea atmosphere. *Journal of Climate*, **24 (3)**, 893–908.

Emanuel, K. A., 1986: An air-sea interaction theory for tropical cyclones. part i: Steady-state maintenance. *Journal of the Atmospheric Sciences*, **43 (6)**, 585–605.

Ffield, A., 2007: Amazon and orinoco river plumes and nbc rings: Bystanders or participants in hurricane events? *Journal of climate*, **20 (2)**, 316–333.

Foltz, G., and M. McPhaden, 2009: Impact of barrier layer thickness on sst in the central tropical north atlantic. *J. Climate.*, **22**, 285–299, doi:10.1175/2008JCLI2308.1.

Greatbatch, R. J., 1984: On the response of the ocean to a moving storm: Parameters and scales. *Journal of physical oceanography*, **14 (1)**, 59–78.

Grodsky, S. A., and Coauthors, 2012: Haline hurricane wake in the amazon/orinoco plume: Aquarius/sacd and smos observations. *Geophysical Research Letters*, **39 (20)**.

Accepted for publication in *Journal of Physical Oceanography*. DOI 10.1175/JPO-D-18-0267.1.

Hernandez, O., J. Jouanno, and F. Durand, 2016: Do the amazon and orinoco freshwater plumes really matter for hurricane-induced ocean surface cooling? *Journal of Geophysical Research: Oceans*, **121 (4)**, 2119–2141.

Jacob, S. D., L. K. Shay, A. J. Mariano, and P. G. Black, 2000: The 3d oceanic mixed layer response to hurricane gilbert. *Journal of Physical Oceanography*, **30 (6)**, 1407–1429.

Leipper, D. F., and D. Volgenau, 1972: Hurricane heat potential of the gulf of mexico. *Journal of Physical Oceanography*, **2 (3)**, 218–224.

Lloyd, I., and G. Vecchi, 2011: Observational evidence for oceanic controls on hurricane intensity. *J. Climate*, **24**, 1138–1153, URL 10.1175/2010JCLI3763.1.

Lukas, R., and E. Lindstrom, 1991: The mixed layer of the western equatorial pacific ocean. *Journal of Geophysical Research: Oceans*, **96 (S01)**, 3343–3357.

Mignot, J., C. de Boyer Montégut, A. Lazar, and S. Cravatte, 2007: Control of salinity on the mixed layer depth in the world ocean: 2. tropical areas. *Journal of Geophysical Research: Oceans*, **112 (C10)**.

Mignot, J., A. Lazar, and M. Lacarra, 2012: On the formation of barrier layers and associated vertical temperature inversions: A focus on the northwestern tropical atlantic. *J. Geophys. Res.*, **117**, URL 10.1029/2011JC007435.

Neetu, S., M. Lengaigne, E. M. Vincent, J. Vialard, G. Madec, G. Samson, M. Ramesh Kumar, and F. Durand, 2012: Influence of upper-ocean stratification on tropical cyclone-induced surface cooling in the bay of bengal. *Journal of Geophysical Research: Oceans*, **117 (C12)**.

Newinger, C., and R. Toumi, 2015: Potential impact of the colored a mazon and o rinoco plume on tropical cyclone intensity. *Journal of Geophysical Research: Oceans*, **120 (2)**, 1296–1317.

Accepted for publication in *Journal of Physical Oceanography*. DOI 10.1175/JPO-D-18-0267.1.

Nguyen, L. T., J. Molinari, and D. Thomas, 2014: Evaluation of tropical cyclone center identification methods in numerical models. *Monthly Weather Review*, **142 (11)**, 4326–4339.

Nolan, D., 2011: Evaluating environmental favorableness for tropical cyclone development with the method of point-downscaling. *J. Adv. Model. Earth Syst.*, **3 (M08001)**, 28, URL 10.1029/2011MS000063.

Onderlinde, M. J., and D. S. Nolan, 2017: The tropical cyclone response to changing wind shear using the method of time-varying point-downscaling. *Journal of Advances in Modeling Earth Systems*, **9 (2)**, 908–931.

Ooyama, K., 1969: Numerical simulation of the life cycle of tropical cyclones. *Journal of the Atmospheric Sciences*, **26 (1)**, 3–40.

Pailler, K., B. Bourles, and Y. Gouriou, 1999: The barrier layer in the western tropical atlantic ocean. *Geophysical Research Letters.*, **26**, 2069–2072, URL 10.1029/1999GL900492.

Price, J., T. Sanford, and G. Forristall, 1994: Forced stage response to a moving hurricane. *J. Phys. Oceanogr.*, **24**, 233–260, URL 10.1175/1520-0485(1994)024⟨0233:FSRTAM⟩2.0.CO;2.

Price, J. F., 1981: Upper ocean response to a hurricane. *Journal of Physical Oceanography*, **11 (2)**, 153–175.

Price, J. F., 1983: Internal wave wake of a moving storm. part i. scales, energy budget and observations. *Journal of Physical Oceanography*, **13 (6)**, 949–965.

Price, J. F., 2009: Metrics of hurricane-ocean interaction: vertically-integrated or vertically-averaged ocean temperature? *Ocean Science*, **5 (3)**, 351–368.

Accepted for publication in *Journal of Physical Oceanography*. DOI 10.1175/JPO-D-18-0267.1.

Price, J. F., R. A. Weller, and R. Pinkel, 1986: Diurnal cycling: Observations and models of the upper ocean response to diurnal heating, cooling, and wind mixing. *J. Geophys. Res.*, **91**, 8411–8427, URL 10.1029/JC091iC07p08411.

Reul, N., Y. Quilfen, B. Chapron, S. Fournier, V. Kudryavtsev, and R. Sabia, 2014a: Multisensor observations of the amazon-orinoco river plume interactions with hurricanes. *J. Geophys. Res.*, **119**, 8271–8295, URL 10.1002/2014JC010107.

Reul, N., and Coauthors, 2014b: Sea surface salinity observations from space with the smos satellite: A new means to monitor the marine branch of the water cycle. *Surveys in Geophysics*, **35 (3)**, 681–722.

Rudzin, J., L. Shay, B. Jaimes, and J. Brewster, 2017: Upper ocean observations in eastern caribbean sea reveal barrier layer within a warm core eddy. *Journal of Geophysical Research: Oceans*, **122 (2)**, 1057–1071.

Rudzin, J. E., L. K. Shay, and W. E. Johns, 2018: The influence of the barrier layer on sst response during tropical cyclone wind forcing using idealized experiments. *Journal of Physical Oceanography*, **(2018)**.

Samson, G., H. Giordani, G. Caniaux, and F. Roux, 2009: Numerical investigation of an oceanic resonant regime induced by hurricane winds. *Ocean Dynamics*, **59 (4)**, 565–586, doi:10.1007/s10236-009-0203-8, URL https://doi.org/10.1007/s10236-009-0203-8.

Shay, L. K., and J. K. Brewster, 2010: Oceanic heat content variability in the eastern pacific ocean for hurricane intensity forecasting. *Monthly Weather Review*, **138 (6)**, 2110–2131.

Shay, L. K., R. L. Elsberry, and P. G. Black, 1989: Vertical structure of the ocean current response to a hurricane. *Journal of physical oceanography*, **19 (5)**, 649–669.

Accepted for publication in *Journal of Physical Oceanography*. DOI 10.1175/JPO-D-18-0267.1.

Shay, L. K., G. J. Goni, and P. G. Black, 2000: Effects of a warm oceanic feature on hurricane opal. *Monthly Weather Review*, **128 (5)**, 1366–1383.

Sprintall, J., and M. Tomczak, 1992: Evidence of the barrier layer in the surface layer of the tropics. *Journal of Geophysical Research.*, **27**, 7305–7316.

Sun, Y., Z. Zhong, L. Yi, Y. Ha, and Y. Sun, 2014: The opposite effects of inner and outer sea surface temperature on tropical cyclone intensity. *Journal of Geophysical Research: Atmospheres*, **119 (5)**, 2193–2208.

Vincent, E. M., K. A. Emanuel, M. Lengaigne, J. Vialard, and G. Madec, 2014: Influence of upper ocean stratification interannual variability on tropical cyclones. *Journal of Advances in Modeling Earth Systems*, **6 (3)**, 680–699.

Wu, C., W. Tu, I. Pun, I.-I. Lin, and M. Peng, 2016: Tropical cyclone-ocean interaction in typhoon megi (2010) - a synergy study based on itop observations and atmosphere-ocean coupled model simulations. *Geophys. Res. Atmos.*, **121**, doi:10.1002/2015JD024198.

Xu, J., and Y. Wang, 2010: Sensitivity of tropical cyclone inner-core size and intensity to the radial distribution of surface entropy flux. *Journal of the Atmospheric Sciences*, **67 (6)**, 1831–1852.

Yablonski, R., and I. Ginis, 2009: Limitation of one-dimensional ocean models for coupled hurricane-ocean model forecasts. *Monthly Weather Review*, **137**, 4410–4419.

Yablonsky, R. M., and I. Ginis, 2012: Impact of a warm ocean eddy's circulation on hurricane-induced sea surface cooling with implications for hurricane intensity. *Monthly Weather Review*, **141 (3)**, 997–1021.

Yan, Y., L. Li, and C. Wang, 2017: The effects of oceanic barrier layer on the upper ocean response to tropical cyclones. *Journal of Geophysical Research: Oceans*, **122 (6)**, 4829–4844.

Accepted for publication in *Journal of Physical Oceanography*. DOI 10.1175/JPO-D-18-0267.1.

LIST OF TABLES

Accepted for publication in *Journal of Physical Oceanography*. DOI 10.1175/JPO-D-18-0267.1.

TABLE 1. Description of Experiments. For each ”Yes”, a suite of simulations was run for the corresponding U_h, initial isothermal layer temperature, and ocean model (a suite indicates 5 ensemble members for OBL0-OBL30, i.e. 20 simulations). In total, 180 simulations were performed.

U_h	$UNFAV, 3DPWP$	$MOD, 3DPWP$	$FAV, 3DPWP$	$MOD, 1DPWP$	$FAV, 1DPWP$
SLOW	Yes	Yes	Yes	Yes	Yes
MEDIUM	Yes	Yes	Yes	No	No
FAST	No	Yes	No	No	No

Accepted for publication in *Journal of Physical Oceanography*. DOI 10.1175/JPO-D-18-0267.1.

TABLE 2. OBLI PMIN (%) mean and standard deviations for the MOD and FAV simulations

		Slow			Medium			Fast		
		OBL12	OBL24	OBL30	OBL12	OBL24	OBL30	OBL12	OBL24	OBL30
UNFAV	Mean	3.73	7.24	15.82	1.25	5.01	6.64	N/A	N/A	N/A
	SD	9.12	9.99	11.52	4.67	9.75	5.54	N/A	N/A	N/A
MOD	Mean	5.08	6.52	12.13	1.67	8.40	8.82	3.43	6.46	6.10
	SD	5.71	6.92	6.88	3.66	3.25	1.86	4.48	4.94	1.57
FAV	Mean	4.51	7.88	10.11	1.13	7.98	9.68	N/A	N/A	N/A
	SD	4.48	5.28	6.68	3.69	4.96	3.86	N/A	N/A	N/A
MOD 1D	Mean	2.02	8.33	13.66	N/A	N/A	N/A	N/A	N/A	N/A
	SD	7.14	4.46	3.41	N/A	N/A	N/A	N/A	N/A	N/A
FAV 1D	Mean	2.77	8.06	11.58	N/A	N/A	N/A	N/A	N/A	N/A
	SD	3.64	5.48	5.48	N/A	N/A	N/A	N/A	N/A	N/A

Accepted for publication in *Journal of Physical Oceanography*. DOI 10.1175/JPO-D-18-0267.1.

LIST OF FIGURES

Accepted for publication in *Journal of Physical Oceanography*. DOI 10.1175/JPO-D-18-0267.1.

Accepted for publication in *Journal of Physical Oceanography*. DOI 10.1175/JPO-D-18-0267.1.

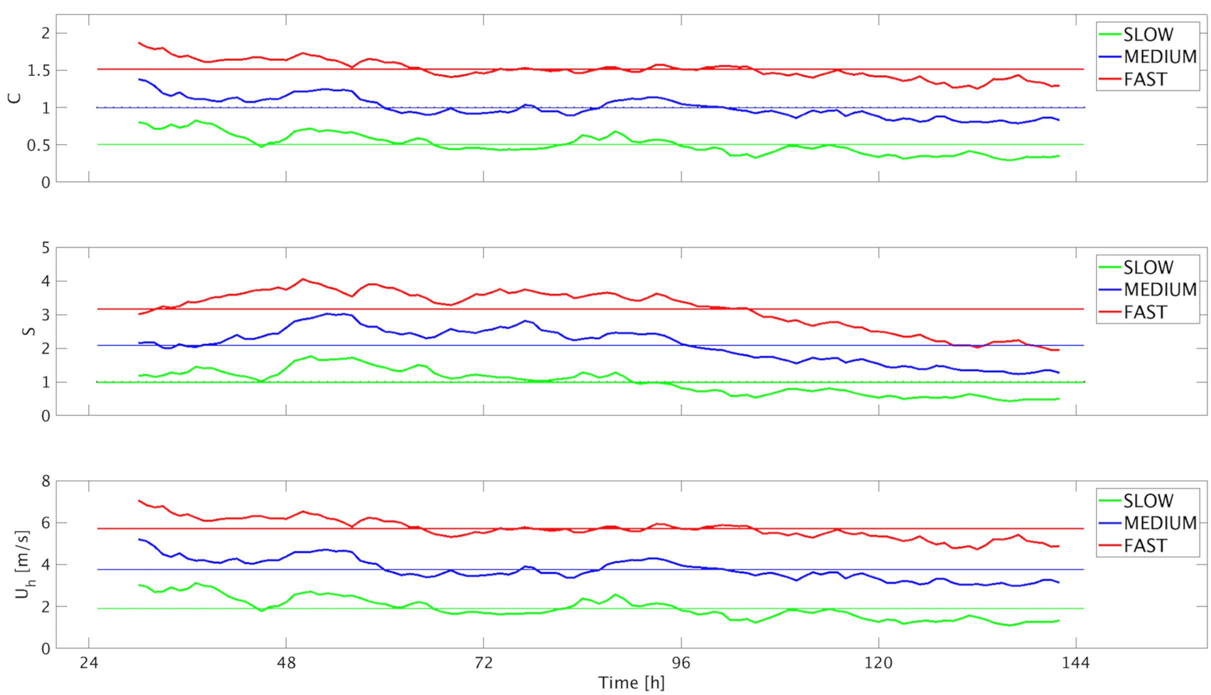

763 FIG. 1. Variations in SLOW (green), MEDIUM (blue), and FAST (red) translation speed for three ensemble
764 members, represented by C (top), S (middle), and U_h (bottom). A five-point running mean is applied. Straight
765 lines indicate the time-averaged values for each.

Accepted for publication in *Journal of Physical Oceanography*. DOI 10.1175/JPO-D-18-0267.1.

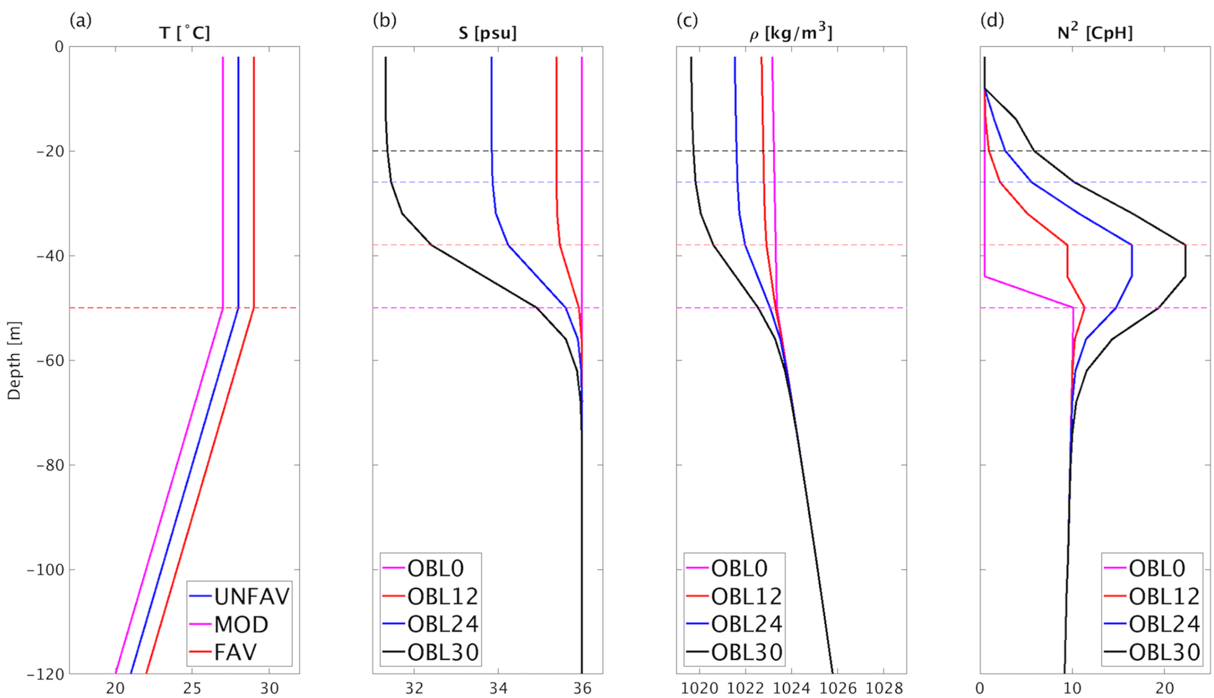

FIG. 2. (a) Temperature (°C), (b) Salinity (psu), (c) density (kg m $^{-3}$), and (d) Brunt-Väisälä frequency (CpH) differences between OBL cases for mixed layer temperatures of 28°C. Dashed lines indicate the ILD in the temperature plot, and the various MLD between each OBL case.

Accepted for publication in *Journal of Physical Oceanography*. DOI 10.1175/JPO-D-18-0267.1.

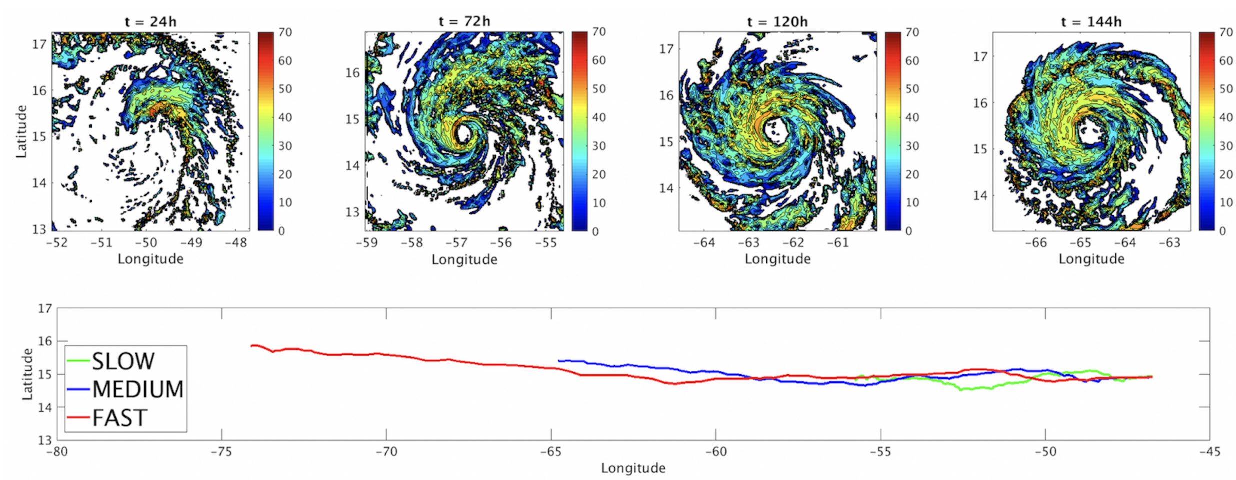

769 FIG. 3. Top: Example evolution of surface reflectivity (dBZ) for a MEDIUM, OBL24 ensemble member from
770 the MOD set. Bottom: Differences in track between example SLOW, MEDIUM, and FAST cases.

Accepted for publication in *Journal of Physical Oceanography*. DOI 10.1175/JPO-D-18-0267.1.

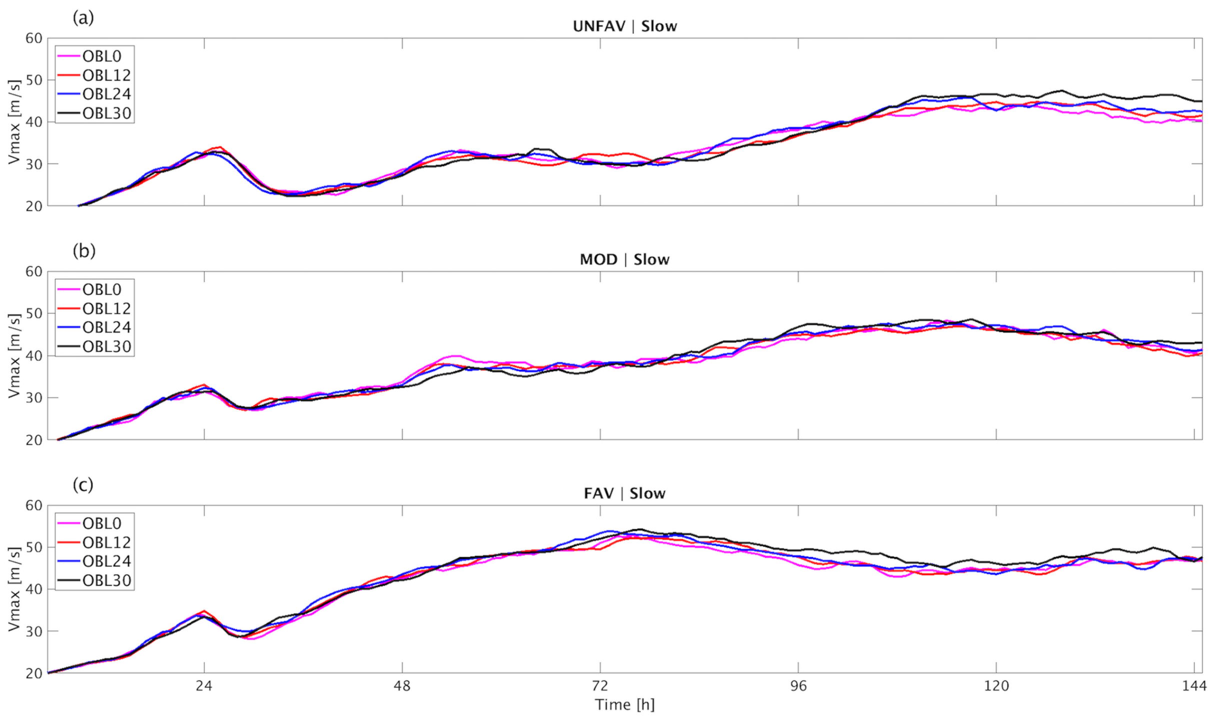

FIG. 4. Ensemble mean maximum velocity for SLOW as a function of time for UNFAV (a), MOD (b), and FAV (c), for each OBL case.

Accepted for publication in *Journal of Physical Oceanography*. DOI 10.1175/JPO-D-18-0267.1.

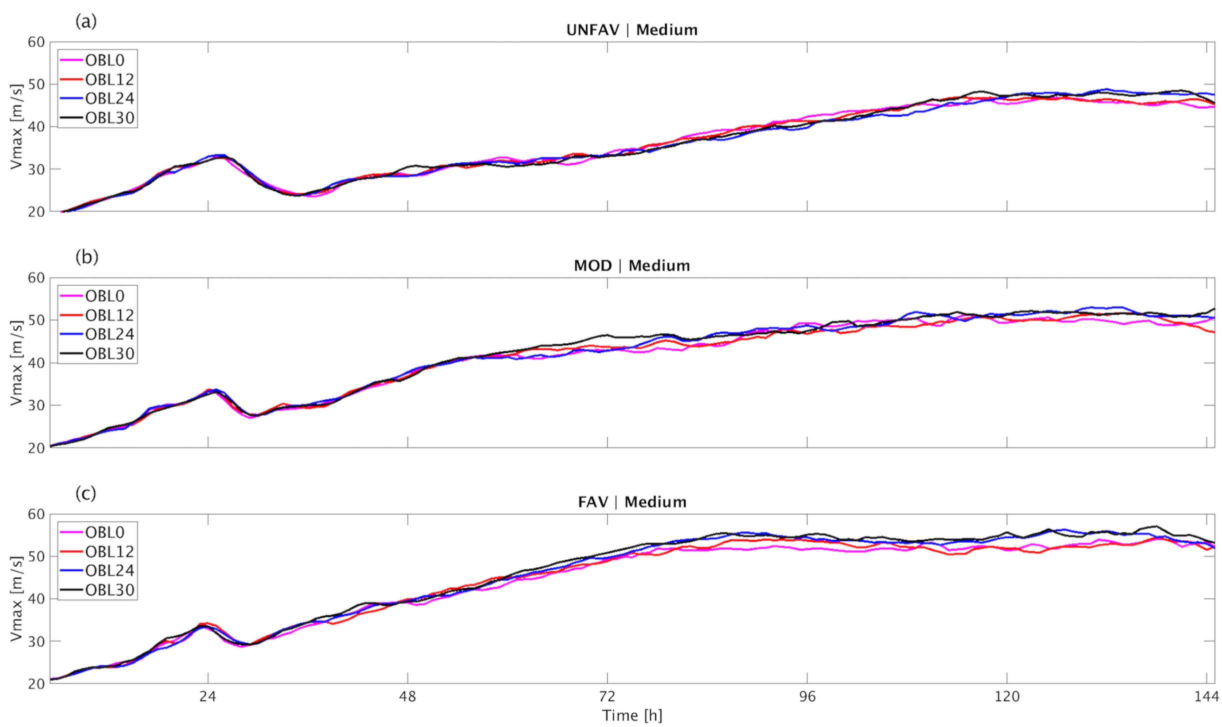

773 FIG. 5. Ensemble mean maximum velocity for MEDIUM as a function of time for UNFAV (a), MOD (b), and
774 FAV (c), for each OBL case.

Accepted for publication in *Journal of Physical Oceanography*. DOI 10.1175/JPO-D-18-0267.1.

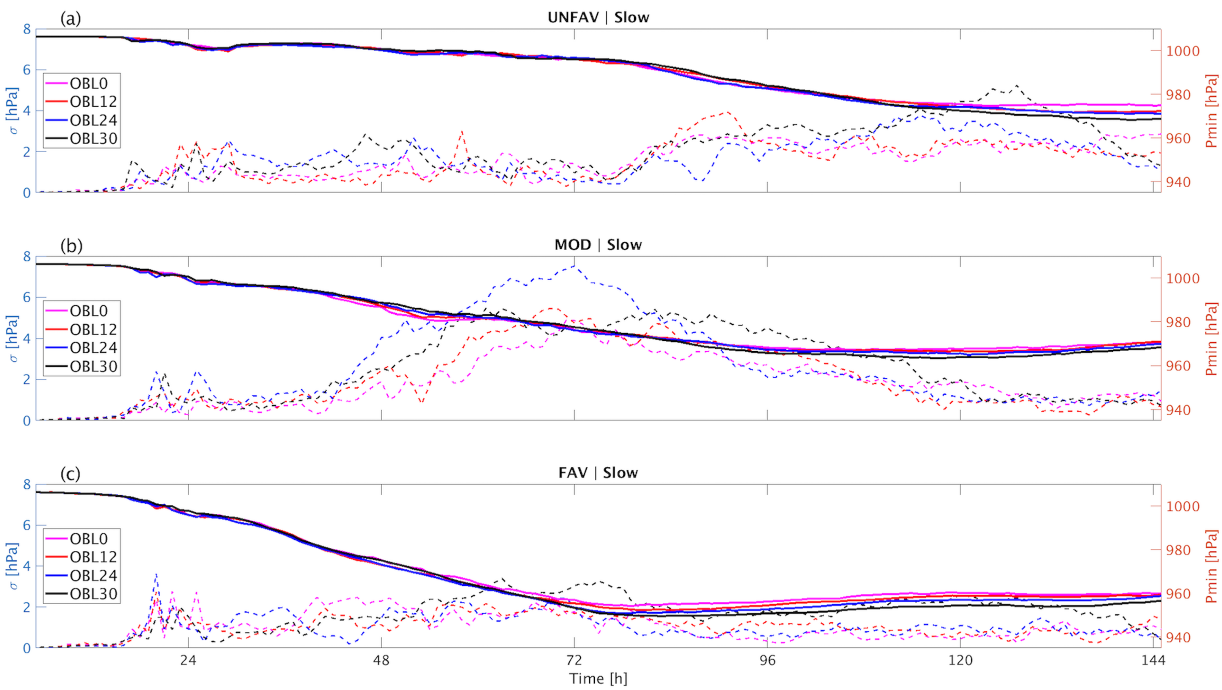

775 FIG. 6. Ensemble mean time series of minimum pressure (solid lines, right axis) for each OBL case for the
776 (a) UNFAV, (b) MOD, and (c) FAV environmental conditions for SLOW. Thin dashed lines (left axis) show the
777 ensemble member standard deviation from the ensemble mean as a function of time.

Accepted for publication in *Journal of Physical Oceanography*. DOI 10.1175/JPO-D-18-0267.1.

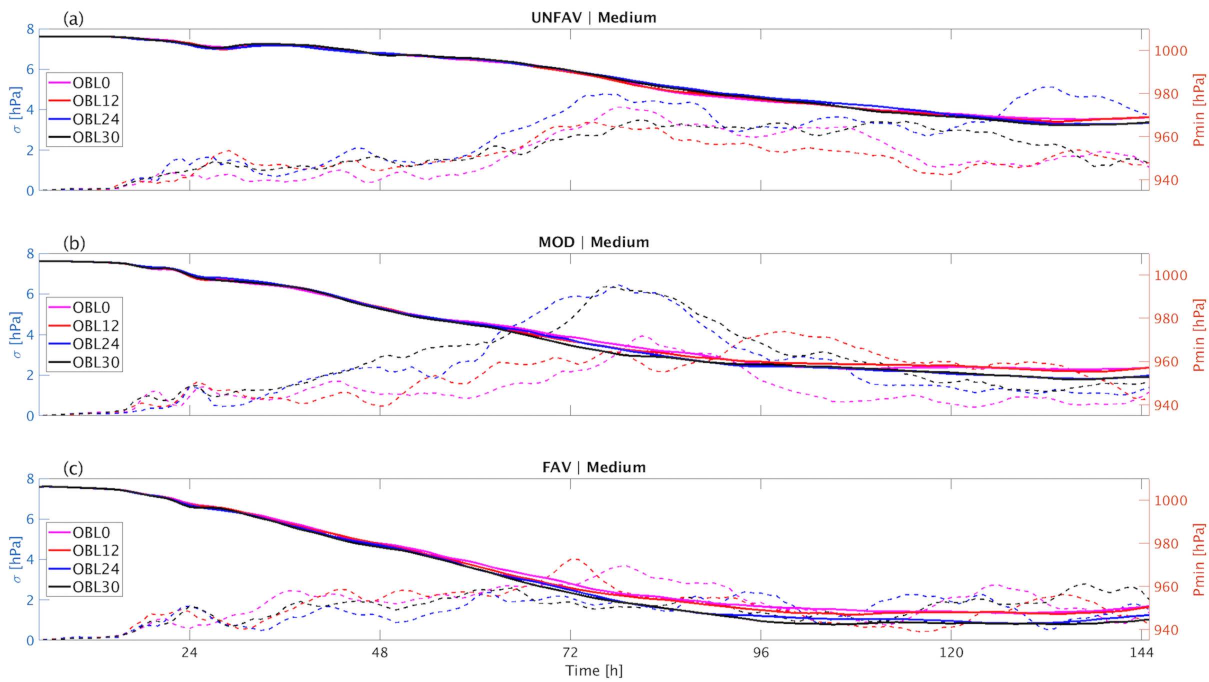

FIG. 7. As in fig. 6 for MEDIUM.

Accepted for publication in *Journal of Physical Oceanography*. DOI 10.1175/JPO-D-18-0267.1.

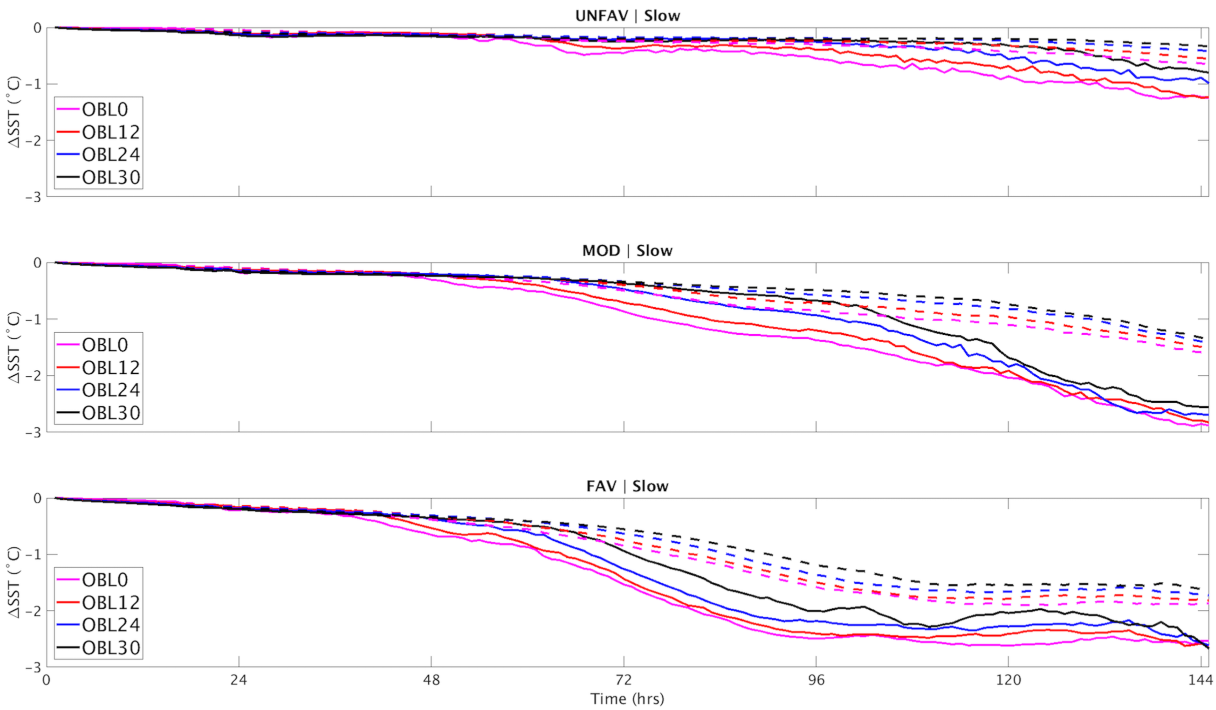

778 FIG. 8. Ensemble mean time series of TC core-averaged ΔSST (°C) for each OBL case for the (top) UNFAV,
779 (middle) MOD, and (bottom) FAV environmental conditions in SLOW. The solid (dashed) lines indicate the
780 average within 60 (200) km of the TC center.

Accepted for publication in *Journal of Physical Oceanography*. DOI 10.1175/JPO-D-18-0267.1.

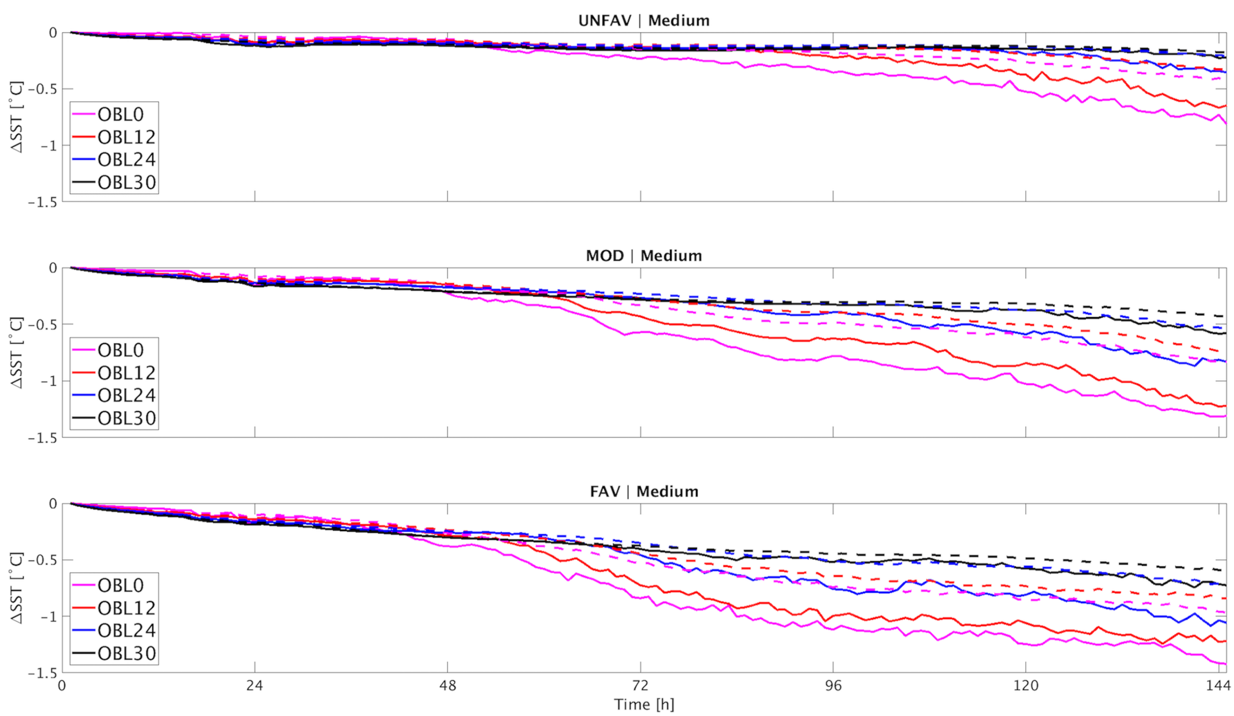

FIG. 9. As in fig. 8, but for MEDIUM. Note the different y-axis used.

Accepted for publication in *Journal of Physical Oceanography*. DOI 10.1175/JPO-D-18-0267.1.

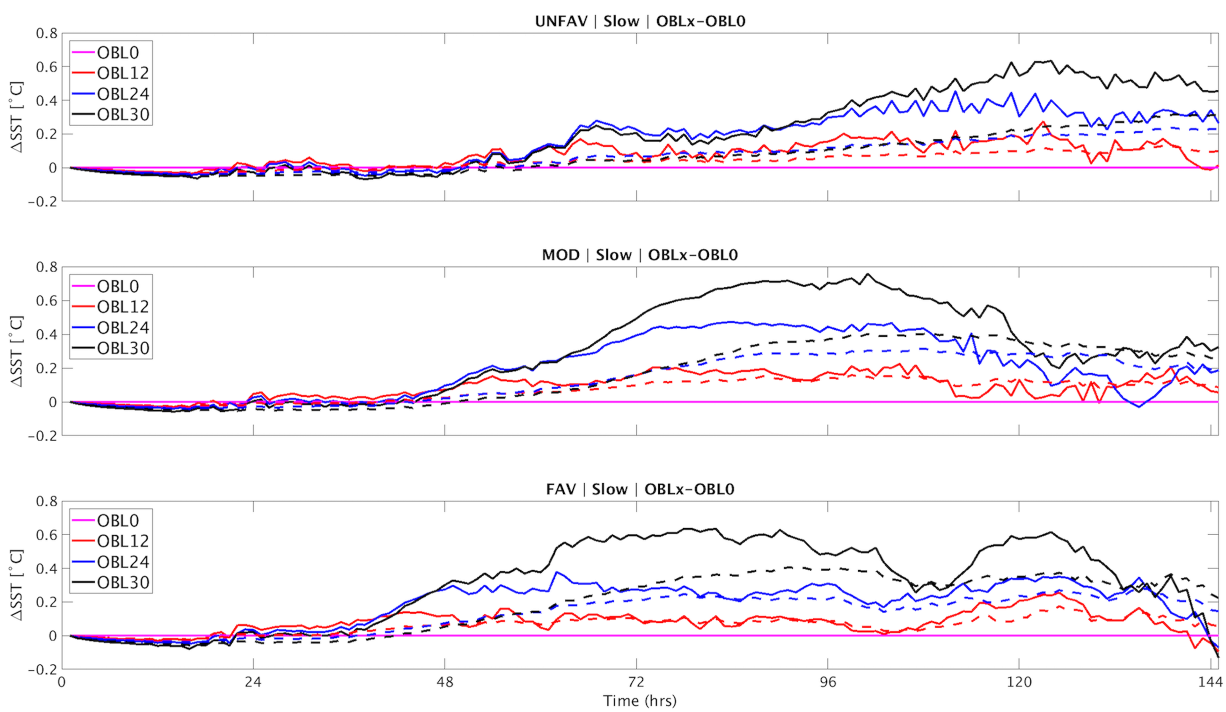

781 FIG. 10. Ensemble mean time series of Δ SST within 60 km of the center for each OBL case, relative to
782 OBL0, for the (top) UNFAV, (middle) MOD, and (bottom) FAV environmental conditions when U_h is slow.

Accepted for publication in *Journal of Physical Oceanography*. DOI 10.1175/JPO-D-18-0267.1.

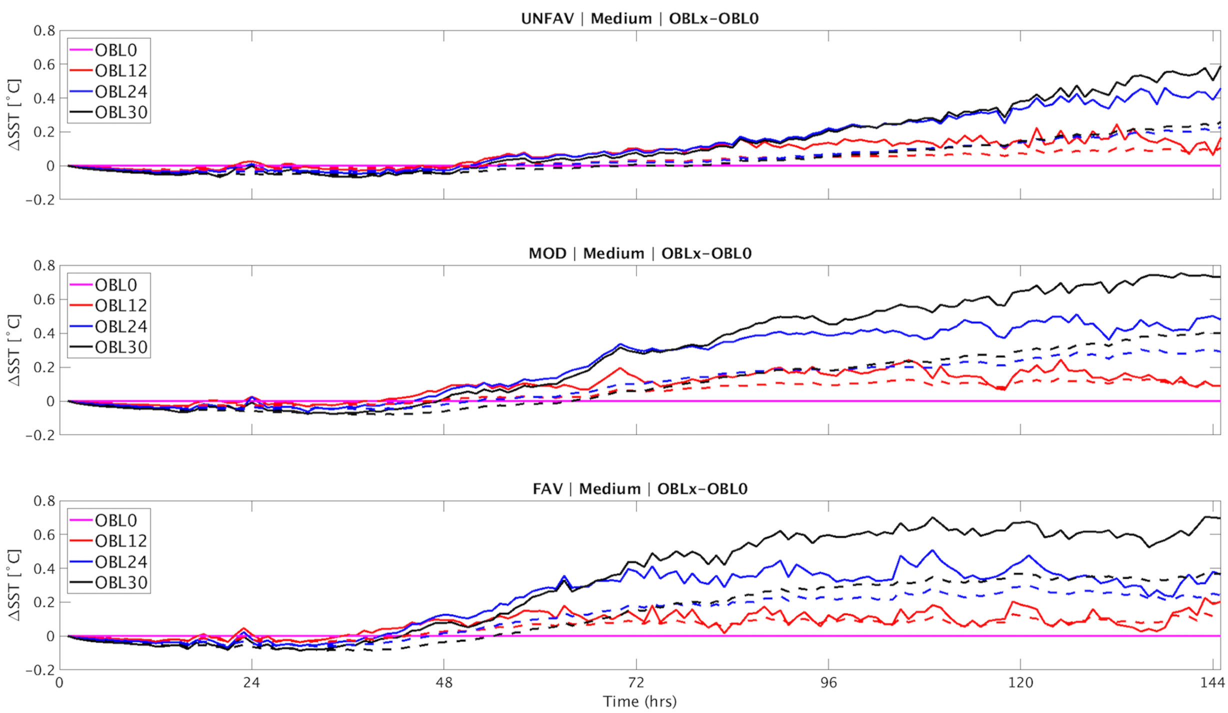

FIG. 11. As in fig. 10, but for MEDIUM.

Accepted for publication in *Journal of Physical Oceanography*. DOI 10.1175/JPO-D-18-0267.1.

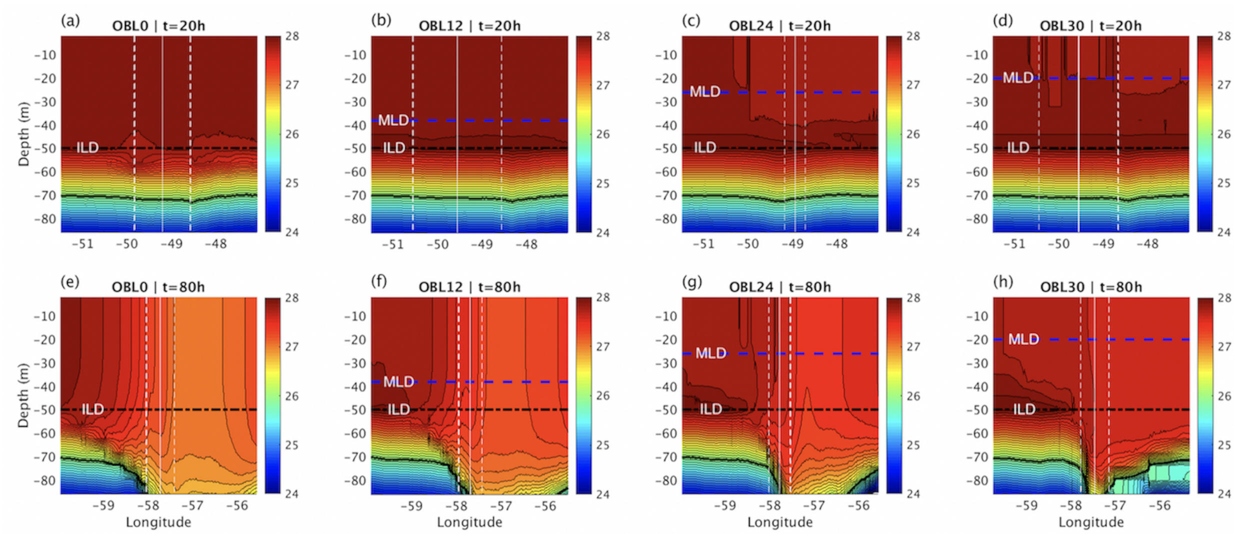

FIG. 12. Ocean temperatures at a constant latitude through the storm center as a function of longitude and depth at $t = 20$ h (a-d) and $t = 80$ h (e-h) for a MEDIUM MOD ensemble member, where (a,e): OBL0, (b,f): OBL12, (c,g): OBL24, (d,h): OBL30. Contours are every 0.1°C . The vertical solid white line indicates the longitude of the TC center, and the white dashed lines indicate 1 RMW ahead of and behind the center. Horizontal blue thick dashed and black dot-dashed mark the initial mixed layer depth/top of halocline (MLD) and isothermal layer depth (ILD), and the solid black contours mark the current 26°C isotherm level for each time.

Accepted for publication in *Journal of Physical Oceanography*. DOI 10.1175/JPO-D-18-0267.1.

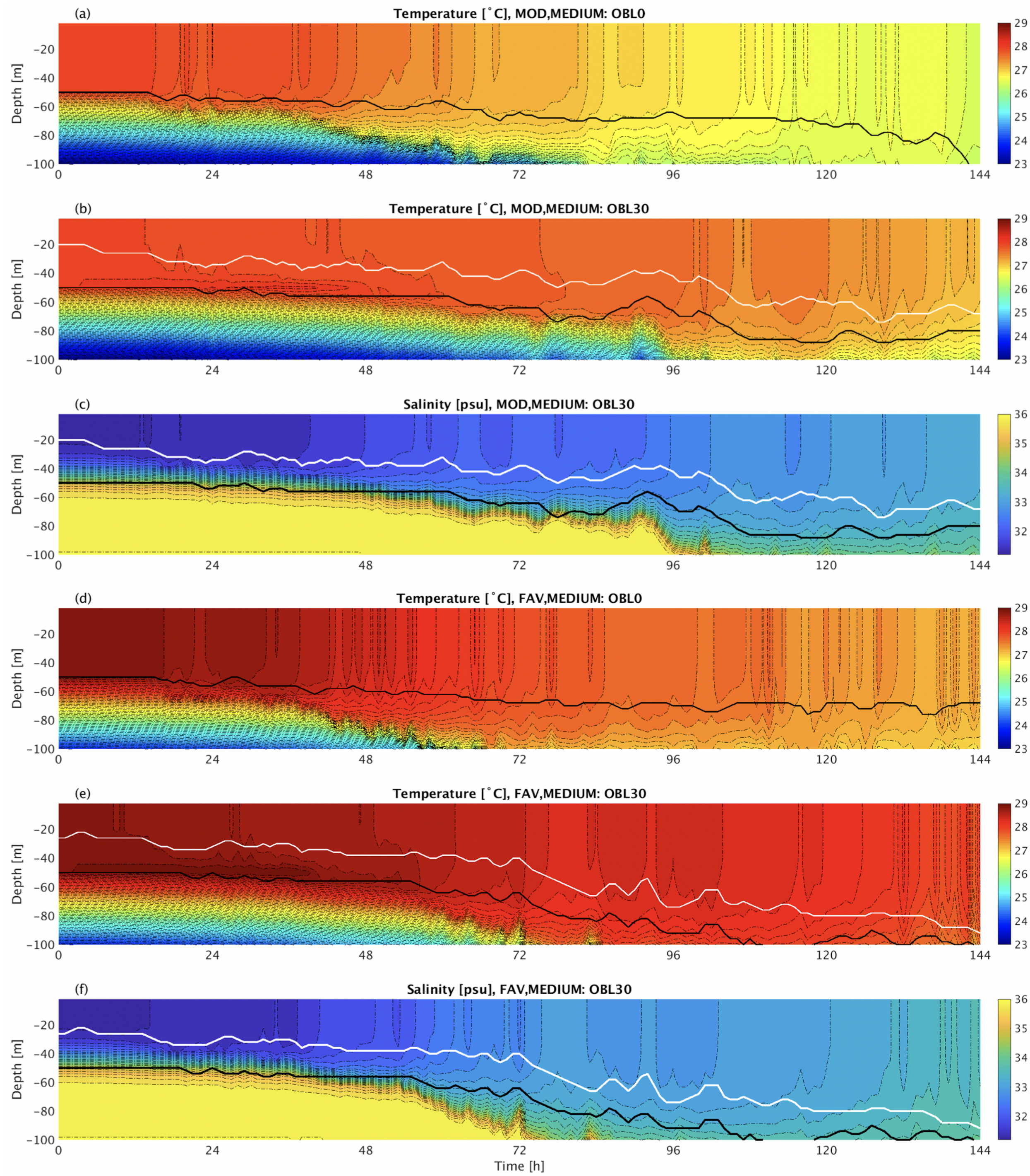

FIG. 13. Hovmöller diagrams of vertical ocean temperature (a,b,d,e; units °C) and salinity (c,f; psu) profiles beneath a point following the TC center, comparing OBL0 (a,d) and OBL30 (b,c,e,f) from MOD, MEDIUM and FAV, MEDIUM ensemble members. Solid black plots show the depth of the isothermal layer (equivalent to the mixed layer depth in the OBL0 case), and the solid white plot shows the depth of the mixed layer for the OBL30 cases.

Accepted for publication in *Journal of Physical Oceanography*. DOI 10.1175/JPO-D-18-0267.1.

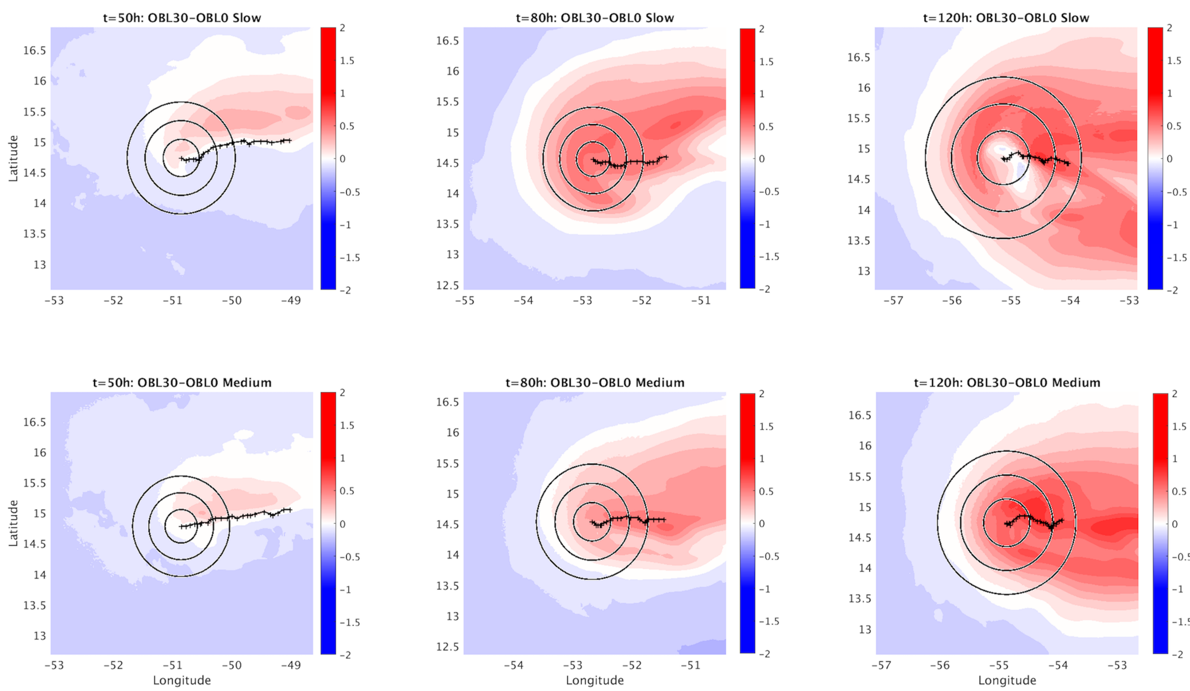

794 FIG. 14. Difference in SST between example MOD SLOW and MEDIUM OBL0 and OBL30 ensemble
795 members at $t = 50, 80$, and 120 h. Red (blue) indicates that the OBL30 SST is warmer (cooler) than the OBL0
796 SST. Black circles indicate 1, 2, and 3 RMW, averaged between the OBL30 and OBL0 cases at each time-step.
797 The plus symbols mark the averaged track between the two OBL cases.

Accepted for publication in *Journal of Physical Oceanography*. DOI 10.1175/JPO-D-18-0267.1.

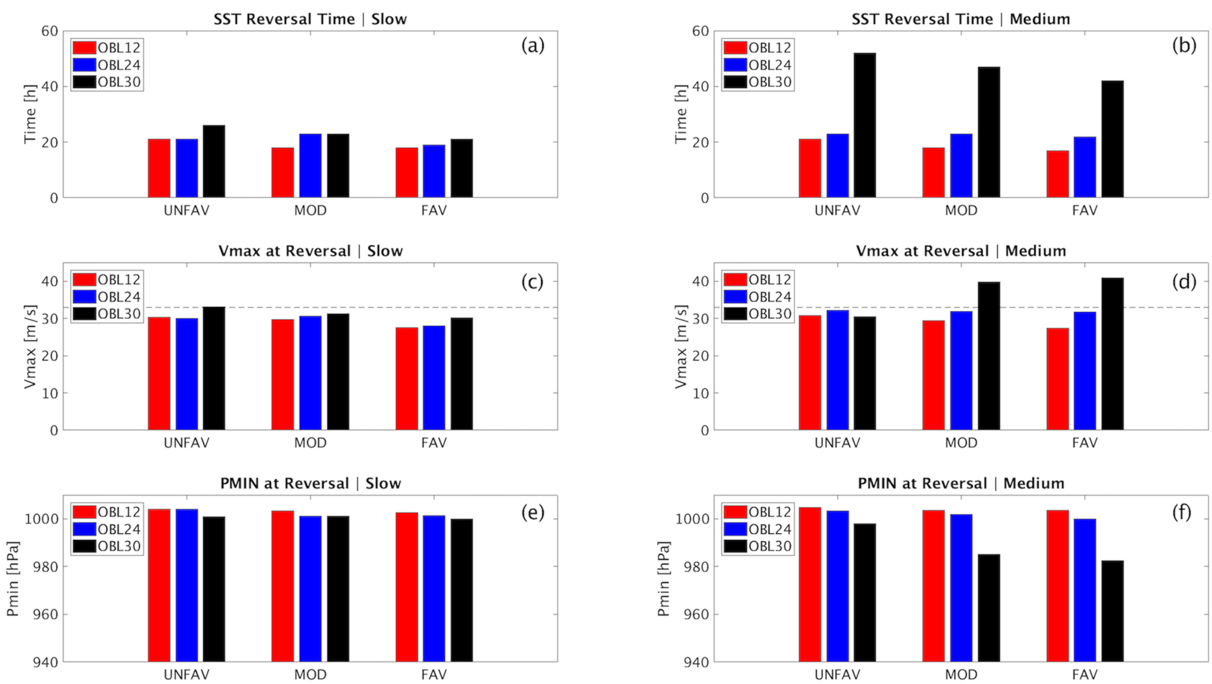

798 FIG. 15. SLOW (a,c,e) and MEDIUM (b,d,f) ensemble means of: (a),(b): Time at which SST cooling for
799 OBL0 exceeds OBLx; (c),(d): VMAX at each time in (a) and (b), with the dashed line marking category 1 status
800 (33 m s^{-1}); PMIN at each time in (a) and (b).

Accepted for publication in *Journal of Physical Oceanography*. DOI 10.1175/JPO-D-18-0267.1.

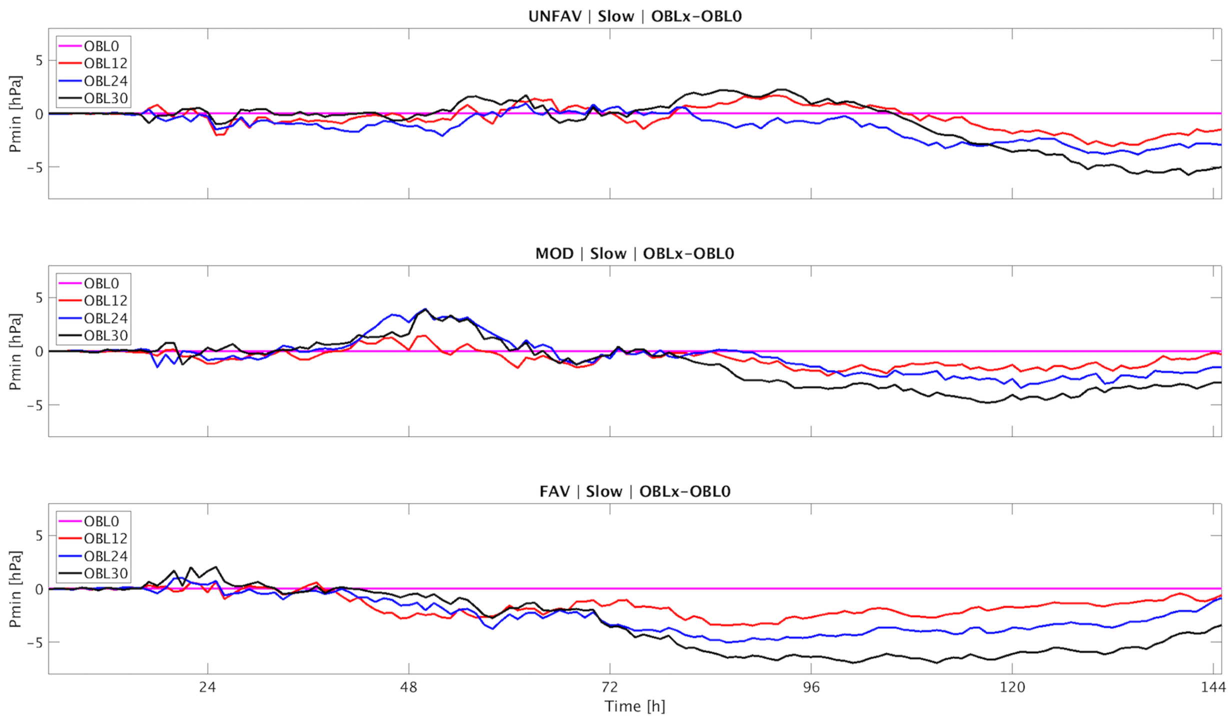

801 FIG. 16. Ensemble mean time series of minimum pressure (hPa) for each OBL case, relative to OBL0, for the
802 (a) UNFAV, (b) MOD, and (c) FAV environmental conditions in SLOW. Here, positive (negative) values indicate
803 that OBLx was weaker (stronger) than OBL0 at a specific time.

Accepted for publication in *Journal of Physical Oceanography*. DOI 10.1175/JPO-D-18-0267.1.

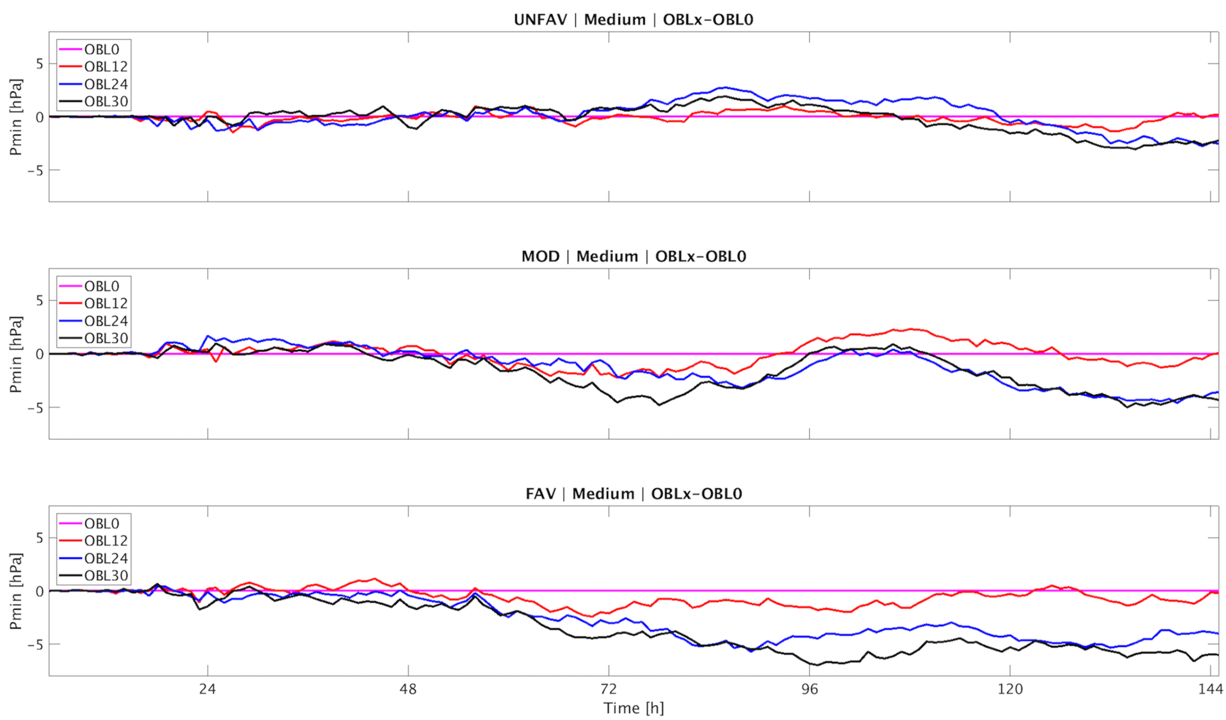

FIG. 17. As in Figure 16, but for MEDIUM.

Accepted for publication in *Journal of Physical Oceanography*. DOI 10.1175/JPO-D-18-0267.1.

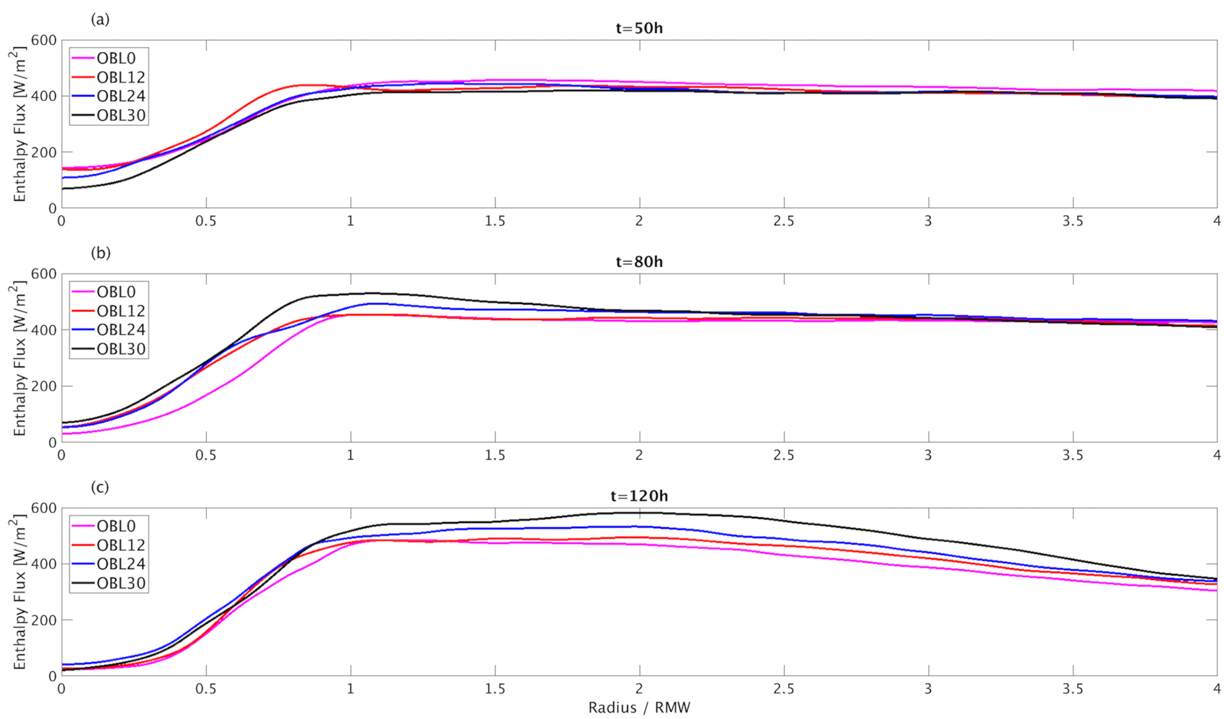

804 FIG. 18. Ensemble mean azimuthally-averaged enthalphy flux (W m^{-2}) for the MOD SLOW U_h set at (a)
805 $t = 50$ h, (b) $t = 80$ h, and (c) $t = 120$ h, as a function of radius (normalized by ensemble mean azimuthally-
806 averaged RMW).

Accepted for publication in *Journal of Physical Oceanography*. DOI 10.1175/JPO-D-18-0267.1.

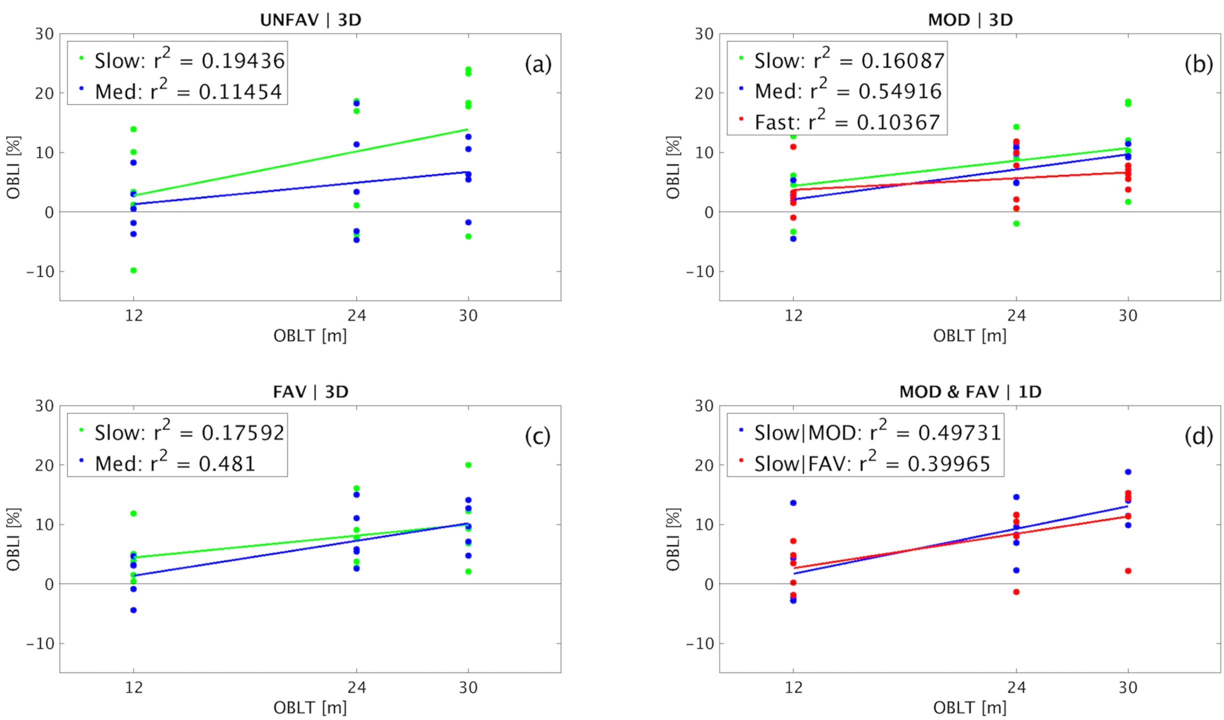

807 FIG. 19. Ensemble member OBLI for (a) UNFAV, (b) MOD, (c) FAV, and (d) MOD and FAV, 1DPWP as a
808 function of OBLT. Linear best fit lines are shown for each U_h, with correlation coefficients provided.

Accepted for publication in *Journal of Physical Oceanography*. DOI 10.1175/JPO-D-18-0267.1.

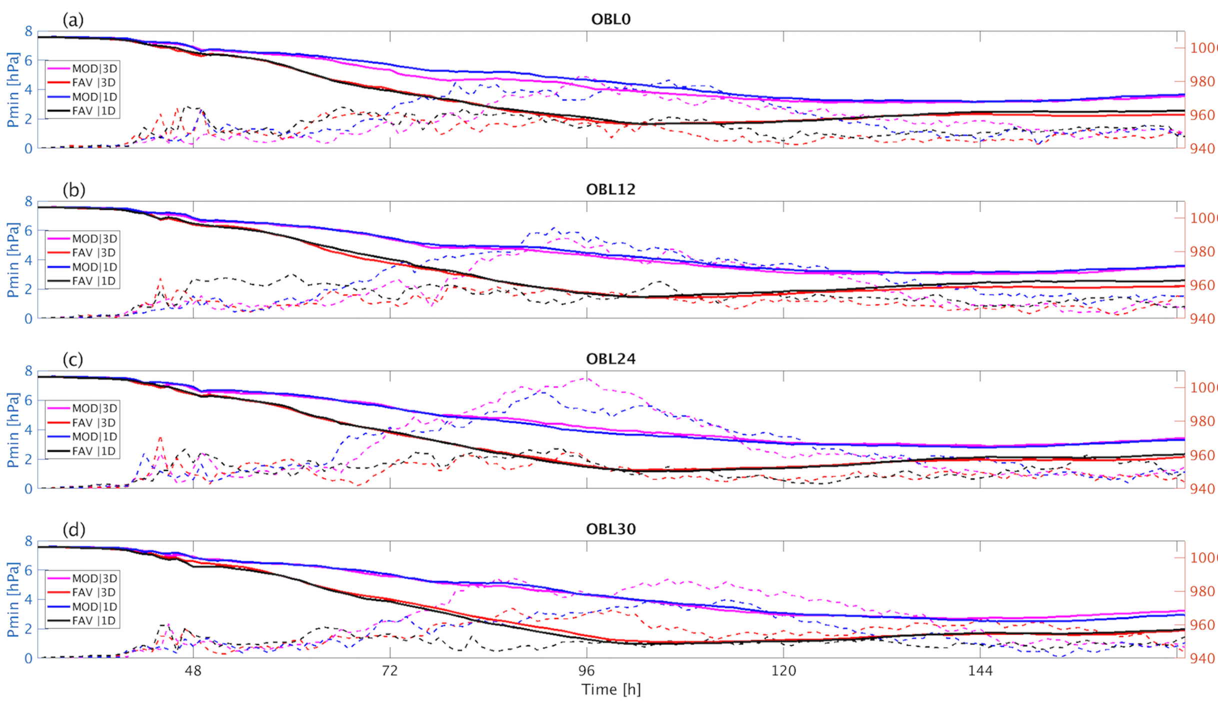

809 FIG. 20. Ensemble mean PMIN (solid) and standard deviation (dashed) time-series for 1D/3D PWP FAV and
810 MOD, for OBL0 (a), OBL12 (b), OBL24 (c), OBL30 (d).

Accepted for publication in *Journal of Physical Oceanography*. DOI 10.1175/JPO-D-18-0267.1.

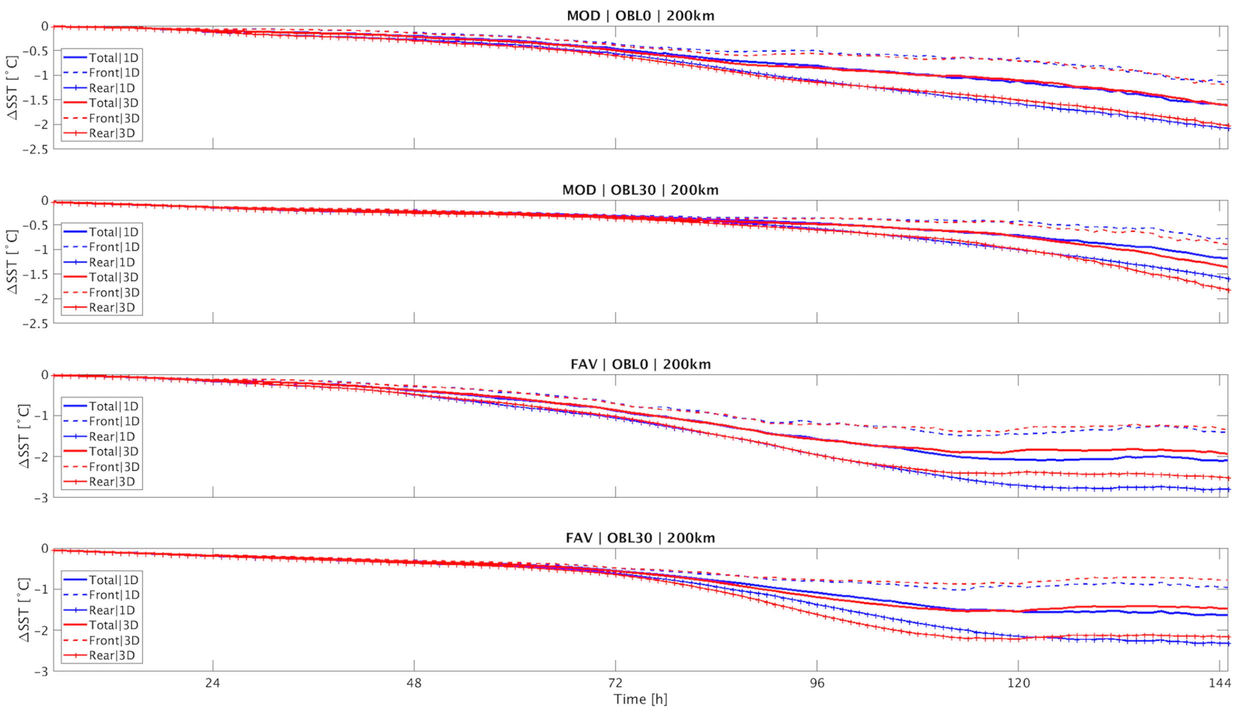

811 FIG. 21. Ensemble mean Δ SST comparing 1D MOD, SLOW and FAV, SLOW to 3D counterparts, averaged
812 within 200 km of the center. Solid blue and red refer to the total Δ SST averages for 1D and 3D, while the dashed
813 and crossed lines show the values for the front and rear two quadrants, relative to the storm motion.

Accepted for publication in *Journal of Physical Oceanography*. DOI 10.1175/JPO-D-18-0267.1.